nature neuroscience

ARTICLES

https://doi.org/10.1038/s41593-019-0468-2

A neural circuit for comorbid depressive symptoms in chronic pain

Wenjie Zhou[1,9], Yan Jin[1,9], Qian Meng[1,9], Xia Zhu[1,9], Tongjian Bai[2], Yanghua Tian[2], Yu Mao[1,2], Likui Wang[2], Wen Xie[3], Hui Zhong[3], Na Zhang[4], Min-Hua Luo[5], Wenjuan Tao[1], Haitao Wang[1], Jie Li[1], Juan Li[1], Ben-Sheng Qiu[1], Jiang-Ning Zhou[1], Xiangyao Li[6], Han Xu[6], Kai Wang[2], Xiaochu Zhang[1], Yong Liu[7], Gal Richter Levin[8], Lin Xu[4] and Zhi Zhang[1*]

Comorbid depressive symptoms (CDS) in chronic pain are a common health problem, but the neural circuit mechanisms underlying these symptoms remain unclear. Here we identify a novel pathway involving 5-hydroxytryptamine (5-HT) projections from the dorsal raphe nucleus (5-HT^{DRN}) to somatostatin (SOM)-expressing and non-SOM interneurons in the central nucleus of the amygdala (CeA). The SOM^{CeA} neurons project directly to the lateral habenula, an area known involved in depression. Inhibition of the 5-HT^{DRN}→SOM^{CeA} pathway produced depression-like behavior in a male mouse model of chronic pain. Activation of this pathway using pharmacological or optogenetic approaches reduced depression-like behavior in these mice. Human functional magnetic resonance imaging data showed that compared to healthy controls, functional connectivity between the CeA-containing centromedial amygdala and the DRN was reduced in patients with CDS but not in patients in chronic pain without depression. These findings indicate that a novel 5-HT^{DRN}→SOM^{CeA}→lateral habenula pathway may mediate at least some aspects of CDS.

Chronic pain and depressive symptoms are frequently encountered clinically, mutually rendering patients more difficult to treat[1–3]. Particularly, depressive symptoms may lead to an excessive duration and intensity of pain[1,4,5]. This tends to create a cycle of pain and depressive symptoms. Finding an effective treatment for CDS is a major challenge in the field[6–8].

The dysfunction of the serotoninergic system has been implicated in both depression and chronic pain disorders[9,10]. In the pain descending pathway, the serotoninergic system is widely thought to modulate pain sensation[11,12]. Many brain regions, such as the thalamus, amygdala, medial prefrontal cortex and insular cortex, are involved in the central regulation of chronic pain[13,14]; most of these nuclei receive ascending 5-HT projections[15,16]. In contrast, little is known about whether or how chronic pain may influence the ascending serotoninergic system that would further modify the central mechanisms of depression. However, several brain regions involved in chronic pain overlap with those involved in depression, such as the amygdala and DRN[17,18]. How chronic pain and depressive symptoms are linked at the level of neuroanatomical substrates is poorly understood. For example, it is unclear whether CDS results from maladaptive changes in the ascending serotonergic system during chronic pain.

The amygdaloid complex is well-known to be relevant to fear learning, anxiety and pain[19–21]. The central nucleus of the amygdala (CeA), referred to as the 'nociceptive amygdala', serves as the main output nucleus for amygdala functions[21]. Highly processed, polymodal information reaches the CeA from the thalamus, cortical areas and brainstem[21–23]. Furthermore, the CeA forms widespread connections with forebrain areas and the brainstem, which have been implicated in mediating fear and mood disorders[22,23]. These studies suggest that the CeA is a probable convergent point of chronic pain and depression. However, the cause-and-effect relationship between the adaptation of CeA circuits and the pathology of CDS is unknown. Based on the evidence linking the amygdala and the serotoninergic system with both pain and depressive symptoms, we investigated the circuit mechanism underlying of CDS by identifying the CeA circuits through which depression-like behaviors in mice are orchestrated by 5-HT under chronic pain conditions.

Combining viral tracing, electrophysiological, optogenetic and chemogenetic methods, we dissected the functional organization of the DRN→CeA circuit and explored the principle of this circuit adaptation in a male mouse model of chronic pain. Furthermore, we employed resting-state functional magnetic resonance imaging (fMRI) to assess whether the circuit identified in the mouse model was relevant to human CDS. Based our findings, we propose a 5-HT^{DRN}→SOM^{CeA}→glutamatergic neurons in lateral habenula (Glu^{LHb}) circuit, the alteration of which is critical for manifesting CDS.

Results

An inhibitory pathway from 5-HT^{DRN} to SOM^{CeA} mediated by 5-HT$_{1A}$Rs. The CeA consists of around 95% GABA (γ-aminobutyric acid) neurons[24]. We first examined the incoming projections onto

[1]Hefei National Laboratory for Physical Sciences at the Microscale, CAS Key laboratory of Brain Function and Disease, University of Science and Technology of China, Hefei, China. [2]Department of Neurology, Department of Anesthesiology and Department of Pain Management, The First Affiliated Hospital of Anhui Medical University, Hefei, China. [3]Department of Psychology, Anhui Mental Health Center, Hefei, China. [4]Key Laboratory of Animal Models and Human Disease Mechanisms, and Laboratory of Learning and Memory, Kunming Institute of Zoology, Chinese Academy of Sciences, Kunming, China. [5]State Key Laboratory of Virology, CAS Center for Excellence in Brain Science and Intelligence Technology, Wuhan Institute of Virology, Chinese Academy of Sciences, Wuhan, China. [6]Key Laboratory of Medical Neurobiology of the Ministry of Health of China, Key Laboratory of Neurobiology of Zhejiang Province, Department of Neurobiology, Zhejiang University School of Medicine, Hangzhou, China. [7]National Laboratory of Pattern Recognition, Institute of Automation, Chinese Academy of Sciences, Beijing, China. [8]Sagol Department of Neurobiology, University of Haifa, Haifa, Israel. [9]These authors contributed equally: Wenjie Zhou, Yan Jin, Qian Meng, Xia Zhu. *e-mail: zhizhang@ustc.edu.cn

the CeA GABAergic neurons by using Cre-dependent retrograde trans-monosynaptic tracing viruses. Cre-dependent helper viruses (AAV-Ef1α-DIO-TVA-GFP and AAV-Ef1α-DIO-RVG) were injected into the CeA of the *glutamic acid decarboxylase 2* (*GAD2*, a gene that encodes a GABA synthetic enzyme)-*Cre* mice. After 3 weeks, rabies virus (RV) (EnvA-pseudotyped RV-ΔG-DsRed) was injected into the same site (Supplementary Fig. 1a). The presence of these helper viruses enabled the rabies virus to spread retrogradely across monosynapses. In addition to the well-characterized CeA inputs from areas such as the basolateral amygdala (BLA), paraventricular thalamus and thalamus (Supplementary Fig. 1b,c), we also identified intensely DsRed-labeled neurons in the DRN (Supplementary Fig. 1d), suggesting that DRN neurons innervate CeA GABAergic neurons. This finding is potentially interesting because the 5-HT system has been implicated in depression disorders, and the most prescribed antidepressants, such as paroxetine, target this system[25,26].

To identify the subtypes of CeA neuron innervated by DRN, we focused on three distinct types of GABAergic interneuron, expressing parvalbumin (PV), calretinin (CR) or somatostatin (SOM), respectively[27]. Confocal microscopic images showed DsRed-labeled neurons in the DRN only in *SOM-Cre* mice (Fig. 1a–c), and not in the *PV-Cre* or *CR-Cre* mice (Supplementary Fig. 1e,f). The DsRed signal was mostly co-localized with the 5-HT neuronal marker tryptophan hydroxylase 2 (TPH2), based on immunofluorescence staining (Fig. 1d,e). To confirm this observation, an adeno-associated virus that expressed Cre-dependent channelrhodopsin-2 (AAV-DIO-ChR2-mCherry) was infused into the DRN of *Pet1-Cre* mice, a mouse line that drives Cre enzyme expression in 5-HT neurons[28]. Four weeks later, we observed numerous mCherry$^+$ fibers in the CeA (Supplementary Fig. 1g). All mCherry$^+$ neurons in the DRN were sensitive to 473 nm light stimuli (Supplementary Fig. 1h), ~95% of which were 5-HT neurons (Supplementary Fig. 1i,j). These data suggest that 5-HT^{DRN} neurons send monosynaptic projections to SOM^{CeA} neurons.

To characterize the functional connections of the 5-HT^{DRN}→SOM^{CeA} pathway, *SOM-Cre* and *Pet1-Cre* mice were crossed with *Ai9* (RCL-tdT) mice[29]. The resulting transgenic mice had red tdTomato-expressing SOM (*SOM-tdTOM*) or 5-HT (*Pet1-tdTOM*) neurons that could be visualized in whole-cell patch-clamp recording in acute brain slices. At a high magnification, we observed that the fibers from the DRN were located close to the proximal dendrites and soma of SOM^{CeA} neurons (Fig. 1f,g). Brief light stimulation of ChR2-containing 5-HT^{DRN} terminals in the CeA reliably elicited a hyperpolarized current (−3.01 ± 0.81 mV) in SOM$^+$ neurons, which was reversed by the application of the 5-HT$_{1A}$ receptor (5-HT$_{1A}$R) antagonist WAY100635 (WAY, Fig. 1h,i). Moreover, immunofluorescence showed that 62.3% of 5-HT$_{1A}$R immunoreactivity was present in SOM^{CeA} neurons (Fig. 1j,k). Of note, the hyperpolarized current was not affected in the presence of the GABA$_A$ receptor antagonist picrotoxin (Supplementary Fig. 2), which is consistent with previous studies[30].

To determine whether such optical manipulations of 5-HT^{DRN} in the CeA are sufficient to affect the activity of SOM$^+$ neurons, we examined the action potential firing rate of SOM^{CeA} neurons and the c-Fos expression after photostimulation of 5-HT^{DRN} terminals. We found that the c-Fos expression was increased after optical inhibition of the 5-HT^{DRN} terminals in the CeA (Supplementary Fig. 3a–c), in which 74.7% of c-Fos positive neurons were co-localized with SOM immunofluorescence (Supplementary Fig. 3d,e). In addition, whole-cell recording in brain slices showed that the action potential firing rate of the SOM^{CeA} neurons was decreased by optical activation of 5-HT^{DRN} terminals, which was abolished by perfusion of WAY (Supplementary Fig. 3f,g).

In contrast, light stimulation of ChR2-containing 5-HT^{DRN} terminals in the CeA reliably induced a depolarized current (3.90 ± 0.51 mV) in SOM$^-$ neurons, which was blocked by the selective 5-HT$_{2A}$ receptor (5-HT$_{2A}$R) antagonist MDL100907 (MDL, Fig. 2a,b). Immunofluorescence showed that 79.3% of 5-HT$_{2A}$R positive neurons were SOM$^-$ neurons (Supplementary Fig. 3h). These responses to optical stimulation were similar to those observed following bath application of 5-HT (Fig. 2c). In addition, optical activation of CeA 5-HT^{DRN} terminals increased the frequency of the miniature inhibitory postsynaptic currents (mIPSCs) in SOM$^+$ neurons, which was reversed by the 5-HT$_{2A}$R antagonist (Fig. 2d). This effect was mimicked by bath perfusion of 5-HT (Fig. 2e).

Taken together, these findings suggest that 5-HT^{DRN} neurons send afferents to SOM^{CeA} neurons, causing hyperpolarization and that SOM$^-$ neurons in the CeA locally innervate and inhibit SOM$^+$ neurons (Fig. 2f).

Disinhibition of the 5-HT^{DRN}→SOM^{CeA} circuit in a mouse model of chronic pain. To assess a possible role of the 5-HT^{DRN}→SOM^{CeA} circuit in CDS, we used the spared nerve injury (SNI)-induced neuropathic pain model and the complete Freund's adjuvant (CFA)-induced inflammatory pain model in mice (Fig. 3a and Supplementary Fig. 4a), which are well-accepted mouse models of chronic pain[31]. Six weeks, but not 2 weeks, after SNI surgery (SNI 6W and SNI 2W, respectively), the mice displayed multiple depression-related behaviors in the routine assays, including the open field test (OFT) (that is, reduced center zone time), the elevated plus maze (EPM) test (reduced open arm time), the sucrose preference test (SPT) (decreased preference) and the tail suspension test (TST) (increased immobility) (Fig. 3b and Supplementary Fig. 4b). Similar behavioral phenotypes were observed in mice at 3 weeks, but not 2 weeks, after CFA injection (CFA 3W and CFA 2W, respectively) (Supplementary Fig. 4c). These results suggest that depressive-like behaviors are reliably induced by these chronic pain models. Because most cases of depression in chronic pain are associated with neuropathic pain, which is clinically difficult to treat[32], the SNI mouse model was employed in the following experiments[33].

Whole-cell recordings were performed in visualized CeA-projecting 5-HT neurons from *Pet1-tdT* mice with CeA infusion of the retrograde tracer CTB-488 (Fig. 3c,d). We found a decrease in the spike number in SNI 6W mice (Fig. 3e), suggesting a decrease in 5-HT^{DRN} neuronal activity in SNI 6W mice. However, these phenotypes were not observed in SNI 2W mice (Fig. 3f). Based on this result, we subsequently investigated whether 5-HT levels were decreased in the CeA. Using in vivo microdialysis high-performance liquid chromatography (HPLC) measurements (Fig. 3g and Supplementary Fig. 4d), we determined that the concentration of 5-HT in the CeA was decreased in SNI 6W mice (0.6244 ± 0.053 ng ml^{-1}) relative to sham-treated mice (1.039 ± 0.161 ng ml^{-1}) (Fig. 3h). Similar results were obtained in CFA mice (Supplementary Fig. 4e).

If the SOM^{CeA} neurons are inhibited by 5-HT^{DRN} inputs, the decrease of the inputs under chronic pain conditions should result in disinhibition of these neurons. We found an increase in the spike number, but not the resting membrane potential, in SOM$^+$ neurons from SNI 6W mice compared with sham mice (Fig. 3i and Supplementary Fig. 4f). Selective inhibition of SOM^{CeA} neurons in SNI 6W *SOM-Cre* mice, using Cre-dependent expression of the chemogenetic inhibitory hM4Di in the CeA and intraperitoneal (i.p.) injection of clozapine-*N*-oxide (CNO), reduced depressive-like behaviors (Fig. 3j,k).

Necessary and sufficient role of the 5-HT^{DRN}→SOM^{CeA} circuit for depressive-like behavior in mice with chronic pain. Given the decreased 5-HT^{DRN}→CeA input observed in the presence of persistent pain, we injected the Cre-dependent excitatory hM3Dq to selectively activate 5-HT^{DRN} neurons in *Pet1-Cre* mice (Fig. 4a,b). We found that i.p. injection of CNO significantly reversed the SNI-induced depressive-like behaviors, and this effect was blocked

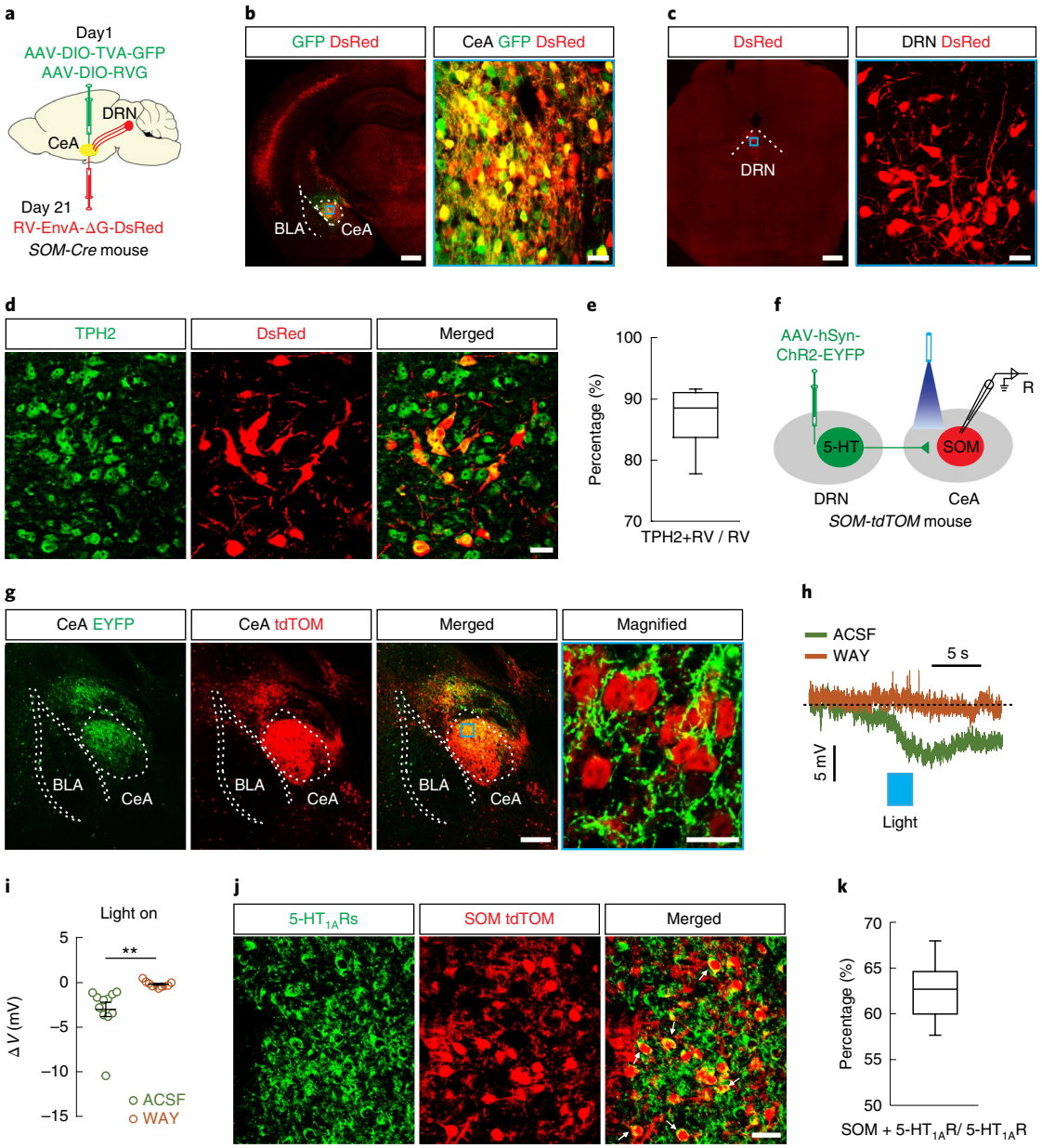

Fig. 1 | Dissection of the 5-HT^{DRN}→SOM^{CeA} circuit. a, Schematic of the *Cre*-dependent retrograde trans-monosynaptic rabies virus tracing strategy. **b**, Typical images of viral expression within the CeA of *SOM-Cre* mice. Starter cells (yellow) co-expressing AAV-DIO-TVA-GFP, AAV-DIO-RVG (green) and RV-EnvA-ΔG-DsRed (red). Scale bars, 500 μm (left) and 50 μm (right). **c**, DsRed-labeled neurons in the DRN traced from the SOM^{CeA}. Scale bars, 500 μm (left) and 50 μm (right). **d**, DsRed signals were co-localized with 5-HT neuronal marker TPH2 immunofluorescence in the DRN. Scale bar, 50 μm. **e**, Percentage of DsRed-labeled neurons that expressed TPH2 in the DRN ($n = 6$ slices from three mice). **f**, Schematic of viral injection in mice and recording configuration in acute slices. **g**, Expression of EYFP in the CeA of *SOM-tdTOM* mice. Scale bars, 250 μm (left) and 50 μm (right). **h**,**i**, Representative traces (**h**) and summarized data (**i**) showing hyperpolarized potentials (V) in SOM^{CeA} neurons evoked by photostimulation of 5-HT^{DRN} terminals in the CeA in the presence of ACSF or 5-HT$_{1A}$ receptor antagonist WAY ($n = 11$ cells, $t_{10} = 3.464$, $P = 0.0061$). **j**,**k**, Representative images (**j**) and percentage (**k**) of SOM^{CeA} neurons co-localized with 5-HT$_{1A}$R immunofluorescence (arrows, right) from *SOM-tdTOM* mice ($n = 6$ slices from three mice). Scale bar, 50 μm. Morphological analyses (**a**–**d**,**g**) were independently repeated five times with similar results obtained. For **e** and **k**, data are shown as box and whisker plots (medians, quartiles (boxes) and ranges minimum to maximum (whiskers)). In **i**, significance was assessed by a two-tailed paired Student's t-test. The data are expressed as the mean ± s.e.m. $^{**}P < 0.01$.

by WAY infusion into the CeA (Fig. 4c). Similar effects were obtained by optical activation of 5-HT^{DRN} terminals in the CeA (Fig. 4d–g and Supplementary Fig. 5a). The activation of this circuit partially reversed the SNI-induced reduction in pain threshold (Supplementary Fig. 5b). Furthermore, in naïve mice, optical inhibition of 5-HT^{DRN} terminals in the CeA produced depressive-like behaviors (Supplementary Fig. 5c–e).

To confirm these findings, we infused the selective 5-HT$_{1A}$R agonist 8-hydroxy-2-(di-*N*-propylamino) tetralin (8-OH) into the CeA and found a profound reversal of depression-related behaviors in SNI mice (Fig. 4h). However, this effect was not obtained by CeA infusion of the selective serotonin reuptake inhibitor (SSRI) paroxetine (Fig. 4h). No change in 5-HT levels in the CeA was detected in mice exposed to chronic restraint stress (CRS) or repeated social

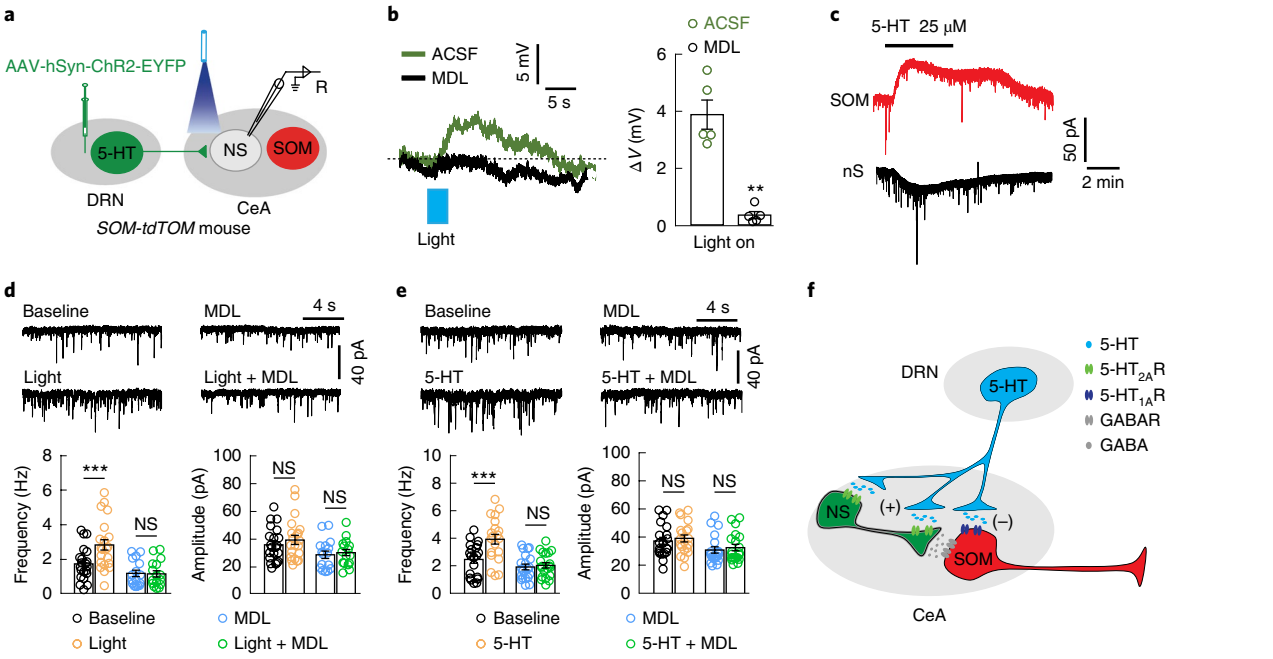

Fig. 2 | 5-HT^{DRN}→Non-SOM^{CeA} circuits. a, Schematic representation showing viral injection in mice and the recording configuration in acute slices. **b**, Representative traces and summarized data showing depolarized potentials in non-SOM^{CeA} (nS) neurons evoked by photostimulation before and after application of 5-HT$_{2A}$R antagonist MDL ($n=5$ cells from three mice, $t_4=6.318$, $P=0.0032$). **c**, Sample traces showing 5-HT hyperpolarized SOM^{CeA} neurons and depolarized nS neurons. The experiment was independently repeated in eight neurons with similar results obtained. **d**,**e**, Sample traces and summarized data showing the effects of photostimulation (**d**, light, $n=21$ cells; light + MDL, $n=16$ cells; frequency, $F_{1,35}=25.82$, $P<0.0001$; amplitude, $F_{1,35}=0.8534$, $P=0.3619$) or bath application of 5-HT (**e**, 5-HT, $n=20$ cells; MDL + 5-HT, $n=20$ cells; frequency, $F_{1,38}=20.1$, $P<0.0001$; amplitude, $F_{1,38}=0.03964$, $P=0.8432$) on mIPSCs recorded from SOM^{CeA} neurons in response to MDL. **f**, A model of long-range and local 5-HT^{DRN}→SOM^{CeA} circuits. The 5-HT^{DRN} neurons send afferents to the CeA, which synapse on SOM neurons, causing hyperpolarization via 5-HT$_{1A}$Rs (−) and on nS neurons, which causes depolarization via 5-HT$_{2A}$Rs (+). In a local CeA circuit, nS neurons inhibit SOM neurons. Significance was assessed by a two-tailed paired Student's *t*-test in **b**, and two-way repeated measures ANOVA with post hoc comparisons between groups in **d**,**e**. The data are presented as the mean ± s.e.m. $^{**}P<0.01$; $^{***}P<0.001$. NS, not significant.

defeat stress (SDS), two rodent models of depression, compared to control mice (Supplementary Fig. 6a–d). Furthermore, optogenetic activation of the 5-HT^{DRN}→SOM^{CeA} circuit did not affect CRS- or SDS-induced depressive-like behaviors (Supplementary Fig. 6e,f). These results show the functional causality of 5-HT^{DRN}→SOM^{CeA} circuit in the development of depressive-like behavior specifically in mice with chronic pain but not in non-pain-related mouse models of depression.

LHb is the output of the 5-HT^{DRN}→SOM^{CeA} circuit for depressive-like behavior in mice with chronic pain. We subsequently aimed to investigate the 5-HT^{DRN}→SOM^{CeA} output circuitry that may mediate depression-like behavior in mice with chronic pain. Following the injection of AAV-DIO-ChR2-mCherry into the CeA of *SOM-Cre* mice, we observed an extremely large number of the mCherry$^+$ fibers in the LHb (Fig. 5a,b), a brain region suggested to be involved in the pathophysiology of depression[34–37] and in other brain regions (Supplementary Fig. 7). To our surprise, optical activation of SOM^{CeA} terminals in the LHb elicited both excitatory postsynaptic currents (EPSCs) and IPSCs in 12 of 25 neurons in brain slices. However, 11 of 25 neurons presented only EPSCs, while two neurons presented only IPSCs (Fig. 5c,d). To dissect the SOM^{CeA}→LHb neuronal organization, we injected Cre-dependent AAV-helper virus and rabies virus into the LHb of *GAD2-Cre* or *CaMKII-Cre* mice. Three weeks later, confocal imaging showed DsRed-labeled neurons in the CeA only in *CaMKII-Cre* and not in *GAD2-Cre* mice (Fig. 5e and Supplementary Fig. 8a,b). Double immunostaining showed that the DsRed-labeled neurons in the CeA co-localized with both SOM and VGLUT2 (Fig. 5f). Additionally, 82.9% of DsRed-labeled neurons co-localized with 5-HT$_{1A}$ receptors, but only 9.6% of neurons co-localized with 5-HT$_{2A}$ receptors (Supplementary Fig. 8c–e). To confirm this result, we injected AAV2/1-hSyn-Cre virus into the CeA, which enabled the Cre enzyme to spread anterogradely and monosynaptically into the soma of neurons, and injected Cre-dependent AAV-DIO-GFP into the ipsilateral LHb (Supplementary Fig. 8f). Three weeks later, numerous GFP-labeled neurons were observed in the LHb, which were co-localized with the VGLUT2 antibody (Supplementary Fig. 8g,h). These results suggest that SOM^{CeA} neurons mainly send glutamatergic projections onto the Glu^{LHb} neurons. In addition, in *CaMKII- tdTOM* mice, whole-cell recording in acute slices showed that the firing rate of Glu^{LHb} neurons was increased after SNI 6W (Fig. 5g). Furthermore, naïve mice displayed depressive-like behaviors following optical activation of SOM^{CeA} terminals in the LHb (Supplementary Fig. 8i, j), whereas optical inhibition of SOM^{CeA} terminals in the LHb of SNI 6W mice alleviated their depressive-like behaviors (Fig. 5h and Supplementary Fig. 8k).

To characterize the connectivity of the 5-HT^{DRN}→SOM^{CeA}→Glu^{LHb} circuit, we took advantage of a new combinatorial strategy that permits direct visualization of these projections (Fig. 6a). We initially injected a retrogradely transported retroAAV (AAV2/2Retro-CMV-bGl-Cre-EGFP) into the LHb that allowed the virus to spread retrogradely into the soma of SOM^{CeA} neurons to express Cre-GFP[38] (Fig. 6b, left). The Cre-dependent retrograde trans-monosynaptic tracing system was subsequently used to infect SOM^{CeA} neurons that expressed the Cre enzyme (Fig. 6b, middle). We visualized numerous DsRed$^+$ cell bodies in the DRN (Fig. 6b, right), which were identified as 5-HT neurons (Fig. 6c).

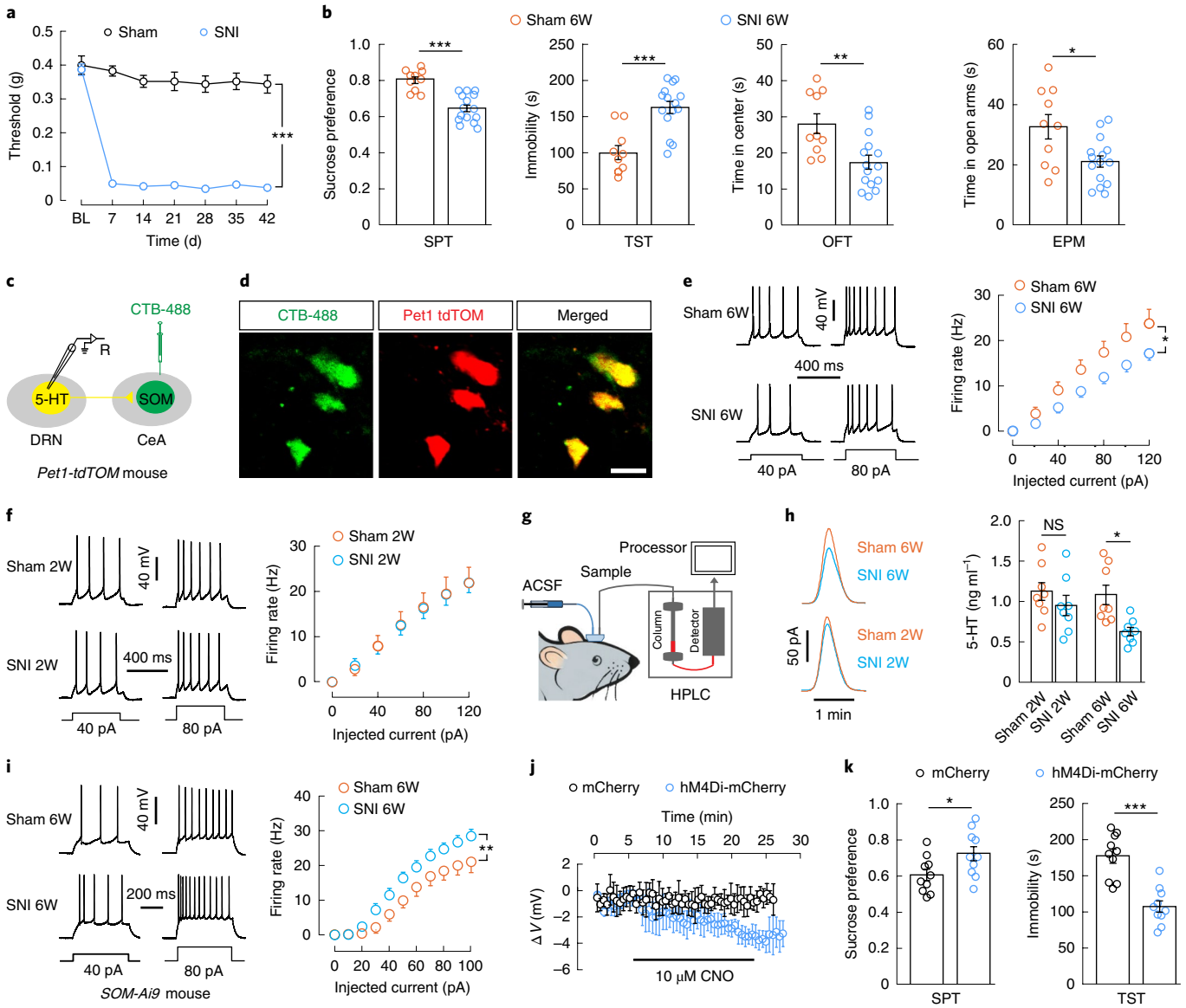

Fig. 3 | Decreased 5-HT^{DRN} inputs to the SOM^{CeA} circuit in mice with chronic pain. a, Time course of SNI-induced sensory pain (sham, $n=10$ mice; SNI, $n=15$ mice; $F_{6,138}=32.04$, $P<0.0001$). **b**, Performance of mice treated with sham or SNI for 6 weeks in SPT, TST, OFT and EPM (sham 6W, $n=10$ mice; SNI 6W, $n=15$ mice; SPT, $t_{23}=5.573$, $P<0.0001$; TST, $t_{23}=4.764$, $P<0.0001$; OFT, $t_{23}=3.274$, $P=0.0033$; EPM, $t_{23}=2.783$, $P=0.0106$). **c**, Schematic of CTB-488 injection in mice and recording configuration in acute slices. **d**, Representative images of 5-HT^{DRN} neurons (yellow) labeled by CTB-488 (green) injected in the CeA of *Pet1-tdTOM* mice. The experiment was independently repeated with similar results in $n=5$ mice. Scale bar, 20 μm. **e**,**f**, Sample traces and statistical data for action potential firing recorded from CeA-projecting 5-HT^{DRN} neurons (yellow cells in **d**) in mice treated with sham or SNI 6W (**e**, sham 6W, $n=24$ cells; SNI 6W, $n=20$ cells; $F_{6,252}=4.223$, $P=0.0005$) or SNI 2W mice (**f**, sham 2W, $n=18$ cells; SNI 2W, $n=17$ cells; $F_{6,198}=0.05696$, $P=0.9992$). **g**, Schematic of microdialysis-HPLC detection in freely moving mice with a probe implanted in the CeA. **h**, Representative traces (left) and summarized data (right) of 5-HT concentration in the CeA from the indicated groups ($n=8$ per group; $F_{3,28}=4.407$, $P=0.0117$). **i**, Representative traces of action potential firing and summarized data from SOM^{CeA} neurons (sham 6W, $n=12$ cells; SNI 6W, $n=14$ cells; $F_{10,240}=3.339$, $P=0.0004$). **j**, Whole-cell recording showing the effect of CNO on AAV-DIO-hM4Di-mCherry or mCherry-expressing SOM^{CeA} neurons ($n=3$ cells from three mice per group). **k**, Behavioral effects of chemogenetic inhibition of SOM^{CeA} neurons with CeA injection of AAV-DIO-hM4Di in *SOM-Cre* mice treated with SNI 6W ($n=10$ per group; SPT, $t_{18}=2.321$, $P=0.0322$; TST, $t_{18}=5.49$, $P<0.0001$). Significance was assessed by two-way repeated measures ANOVA with post hoc comparisons between groups in **a**,**e**,**f**,**i**, two-tailed unpaired Student's *t*-test in **b**,**k** and ordinary one-way ANOVA with post hoc comparison between groups in **h**. The data are expressed as the mean ± s.e.m. $^*P<0.05$, $^{**}P<0.01$, $^{***}P<0.001$.

To assess the functional synaptic connectivity of the 5-HT^{DRN}→SOM^{CeA}→Glu^{LHb} circuit, we injected CTB-488 into the LHb to label LHb-projecting SOM^{CeA} neurons and injected AAV-hSyn-ChR2-mCherry into the DRN of *SOM-tdTOM* mice for slice recording (Fig. 6d,e). Similar to the findings in SOM^{CeA} neurons with 5-HT^{DRN} inputs (see Fig. 1h,i), photostimulation of 5-HT^{DRN} fibers in the CeA elicited a hyperpolarization in the CTB-488-labeled SOM$^+$ neurons (−1.33 ± 0.39 mV) and this effect was reversed by application of WAY (Fig. 6f). Notably, the excitability of these SOM$^+$ neurons was increased in slices from SNI 6W mice (Fig. 6g). Furthermore, the membrane currents of CTB-488-labeled SOM^{CeA} neurons (10/10) were not affected following perfusion of the 5-HT$_{2A}$R antagonist MDL (Fig. 6h). Together, these results identify long-range and local 5-HT^{DRN}→SOM^{CeA}→Glu^{LHb}

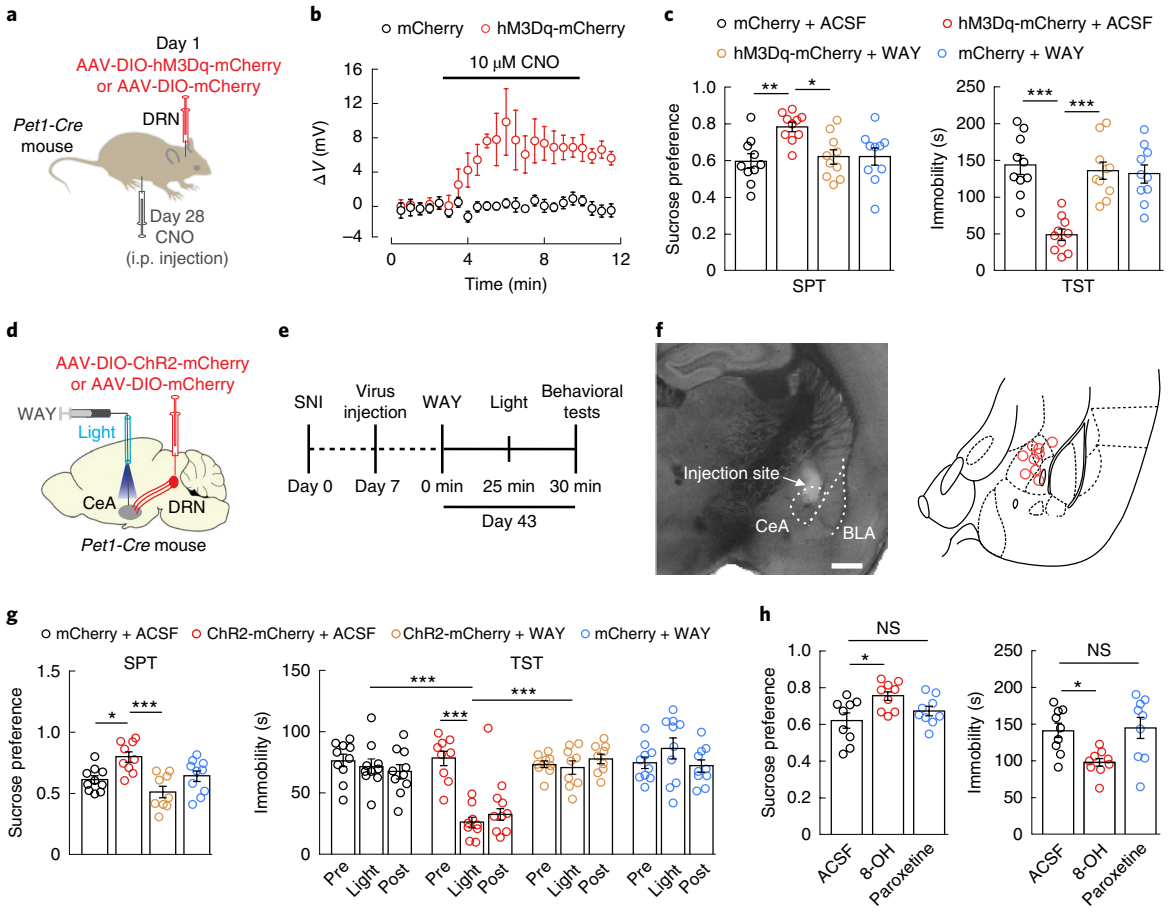

Fig. 4 | Activation of the 5-HT^{DRN}→SOM^{CeA} circuit reduces depressive-like behavior in mice with chronic pain. a, Schematic of chemogenetics. **b**, Whole-cell recording from acute slices showing effect of CNO on AAV-DIO-hM3Dq-mCherry- or mCherry-expressing neurons ($n=3$ cells from three mice per group). **c**, Behavioral effects of the chemogenetic activation of 5-HT^{DRN} neurons in response to WAY ($n=10$ mice per group; SPT, $F_{3,36}=5.478$, $P=0.0033$; TST, $F_{3,36}=15.61$, $P<0.0001$). **d**, Schematic of viral injection and cannula implantation. **e**, Timeline of optogenetic experiments. **f**, A representative image (left) and drawing of optical fiber injection sites (right). Scale bar, 500 μm. **g**, Behavioral effects of optogenetic activation of 5-HT^{DRN} terminals in the CeA in response to WAY (mCherry + ASCF and mCherry + WAY, $n=10$ mice per group; ChR2 + ACSF and ChR2 + WAY, $n=9$ mice per group; SPT, $F_{3,34}=7.86$, $P=0.0004$; TST, $F_{6,68}=10.42$, $P<0.0001$; pre versus light post hoc comparison, ChR2 + ACSF, $P<0.0001$). **h**, Behavioral effects of CeA infusion of 8-OH or paroxetine in SNI 6W mice ($n=9$ mice per group; SPT, $F_{2,24}=4.58$, $P=0.0207$; TST, $F_{2,24}=5.865$, $P=0.0084$). Significance was assessed by ordinary one-way ANOVA with post hoc comparisons between groups in **c**,**g** (SPT), **h**, and two-way repeated measures ANOVA with post hoc comparison between groups in **g** (TST). The data are expressed as the mean ± s.e.m. $^*P<0.05$; $^{**}P<0.01$; $^{***}P<0.001$.

circuits (Supplementary Fig. 9) that are part of a disinhibitory circuit that may underlie CDS in humans.

Decreased functional connectivity between DRN and centromedial amygdala in patients with CDS. Next, we employed resting-state fMRI to assess whether the neural circuit mechanisms for depressive-like behavior in mice with chronic pain may also play a part in CDS in humans. Based on connectivity-based parcellation, the amygdala nucleus in humans was divided into three main groups: superficial, laterobasal and centromedial[39] (Supplementary Fig. 10a). The CeA likely makes up at least a portion of the centromedial region in the majority of humans[40]. The amygdala and centromedial amygdala (CM) were defined according to previous research[39]. We focused on the right CM first. Compared with depressed patients with no chronic pain, patients with CDS showed reduced functional connectivity between the right CM and many brain regions, including the DRN (Supplementary Fig. 10b and Supplementary Table 1). Notably, functional connectivity of the DRN–CM pathway was decreased only in patients with CDS (Supplementary Fig. 10c) and not in depressed patients without pain or in patients in chronic pain without depression, compared with healthy volunteers (Supplementary Fig. 10d–f). Furthermore, functional connectivity of this pathway in patients with CDS was negatively correlated with the Hamilton Depression Rating Scale score (Supplementary Fig. 10g,h), which is a widely used depression assessment scale. CDS was not associated with reduced functional connectivity between the right amygdala and DRN or between the left CM and DRN (Supplementary Fig. 11). These results suggest a link between DRN–CM connectivity and depressive symptoms in patients with chronic pain.

Discussion

Treatments such as SSRIs for patients with CDS are far from satisfactory[41,42], suggesting that a unique circuit mechanism is involved in CDS. Consistent with this notion, we demonstrated that CeA infusion of paroxetine had no effect on the depressive-like behavior in a mouse model of chronic pain. In marked contrast, the activation of 5-HT$_{1A}$Rs in the CeA reduced those behaviors, indicating a role for the 5-HT^{DRN}-SOM^{CeA} circuit in chronic pain-induced depressive-like behavior and, possibly, CDS. It is assumed that SSRIs regulate 5-HT systems in the whole brain through at least 14 5-HT receptor subtypes[43] and thus, the global SSRI actions on multiple

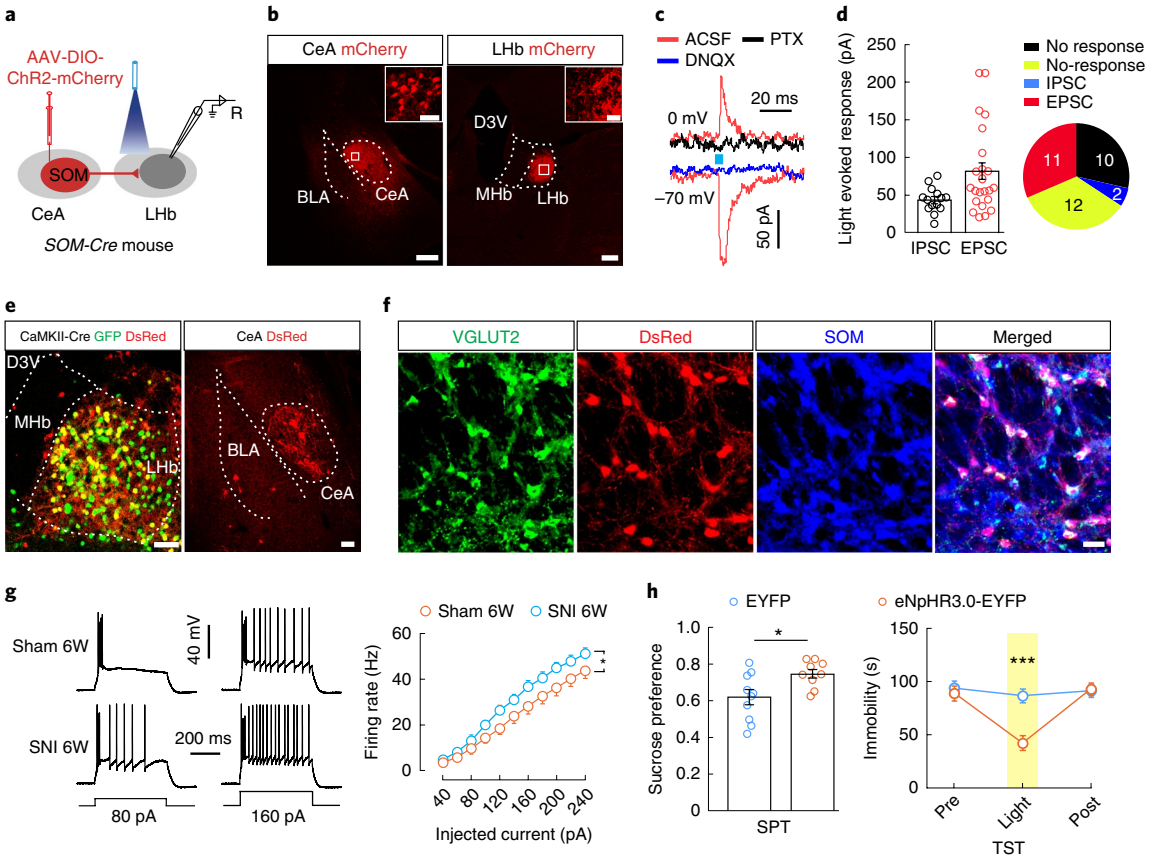

Fig. 5 | Increased SOM^{CeA} inputs to the Glu^{LHb} circuit in in mice with chronic pain. a, Schematic of viral injection in mice and recording configuration in acute slices. **b**, Representative images of viral expression in the CeA (left) and mCherry signals in the LHb (right). D3V, dorsal third ventricle. Scale bars, 50 μm (upper) and 300 μm (bottom). **c**,**d**, Sample traces (**c**) and statistical charts (**d**) showing the light-evoked synaptic responses recorded from LHb neurons ($n=34$ cells) after optical activation of SOM^{CeA} terminals. **e**, Representative images of viral expression within the LHb of *CaMKII-Cre* mice (left) and DsRed signals in the CeA (right). Scale bars, 100 μm. **f**, Representative images of the DsRed-labeled neurons in the CeA that co-localize with VGLUT2 and SOM. Scale bar, 50 μm. **g**, Representative traces (left) of action potential firing and summarized data (right) recorded from Glu^{LHb} neurons (sham 6W, $n=17$ cells; SNI 6W, $n=22$ cells; $F_{10,370}=2.197$, $P=0.0175$). **h**, Behavioral effects of optical inhibition of SOM^{CeA} terminals in the LHb of SNI 6W *SOM-Cre* mice with CeA injection of AAV-DIO-eNpHR3.0-EYFP (eNpHR3.0-EYFP) or control virus EYFP (eNpHR3.0-EYFP, $n=9$; EYFP, $n=10$; SPT, $t_{17}=2.632$, $P=0.0175$; TST, $F_{2,34}=7.809$, $P=0.0016$; eNpHR3.0-EYFP, pre versus light post hoc comparison, $P<0.0001$). Morphological analyses (**b**,**e**,**f**) were independently repeated with similar results in $n=5$ mice. Significance was assessed by two-way repeated measures ANOVA with post hoc comparisons between groups in **g**,**h** (TST) and two-tailed unpaired Student's *t*-test in **h** (SPT). The data are presented as the mean ± s.e.m. $^*P<0.05$; $^{***}P<0.001$.

5-HT receptors, not only on 5-HT$_{1A}$Rs that are critical for depression-related behaviors in chronic pain[44], are probably not effective in treating patients with CDS. In fact, the exact targets for SSRI antidepressants remain elusive. Thus, individual 5-HT receptors, such as 5-HT$_{1A}$Rs, would provide opportunities for the development of new antidepressants for CDS.

The advantage of studying the neural circuit of a disorder is the ability to reveal the convergence point of drug actions and pathological behavioral consequences. We propose a hypothesis for the neural circuit mediating CDS in which persistent pain causes disinhibition of the 5-HT^{DRN}→SOM^{CeA} circuit via 5-HT$_{1A}$Rs in SOM^{CeA} neurons, and the resulting activation of LHb neurons induce depression symptoms. CDS has been found to occur in a state-dependent manner[45], accompanied by a decrease of 5-HT in the CeA and a gradual increase of SOM^{CeA} neuronal activity. It appears that the duration of pain is important for the emergence of depressive problems from our animal studies, as the mice displayed depressive-like behavior at 6 weeks after SNI surgery. This behavioral outcome may be attributed to the dynamic network activity during progressive pain. Adaptations of the 5-HT^{DRN}→SOM^{CeA} circuit in SNI 6W mice, which alter the activity of the LHb, prime the development of depressive-like behavior. In addition, we found that activating the 5-HT^{DRN}→SOM^{CeA} circuit alleviated depressive-like behavior in mice exposed to chronic pain but not in mice exposed to chronic stress, suggesting that this circuitry may be specifically recruited under chronic pain conditions. This is supported by our human fMRI results, in which the functional connectivity between DRN and CM was decreased in patients with CDS but not in depressed patients without chronic pain or in patients with chronic pain without depression. Based on the data from animals and humans, this research provides a cross-species translational study on the behavioral functions of this circuitry.

The DRN-containing brainstem is a crucial relay for carrying nociceptive signals to higher brain centers. However, how adaptation of the ascending 5-HT^{DRN} system may contribute to CDS remains elusive. The serial organization of the CeA microcircuit suggests that the balance of SOM$^+$ excitation is fine-controlled, at least in part, by 5-HT^{DRN} inputs. The 5-HT^{DRN} mediates the inhibition of SOM$^+$ neurons predominantly through a hyperpolarizing process via postsynaptic 5-HT$_{1A}$Rs, whereas synapses onto SOM$^-$ CeA neurons probably exert excitatory effects via 5-HT$_{2A}$Rs. Under persistent pain conditions, the hyperactivity of SOM^{CeA} neurons is driven by dual disinhibition; that is, through both direct weakening of presynaptic 5-HT^{DRN} inputs and reduction in local SOM$^-$ neuronal function. In addition, parallel

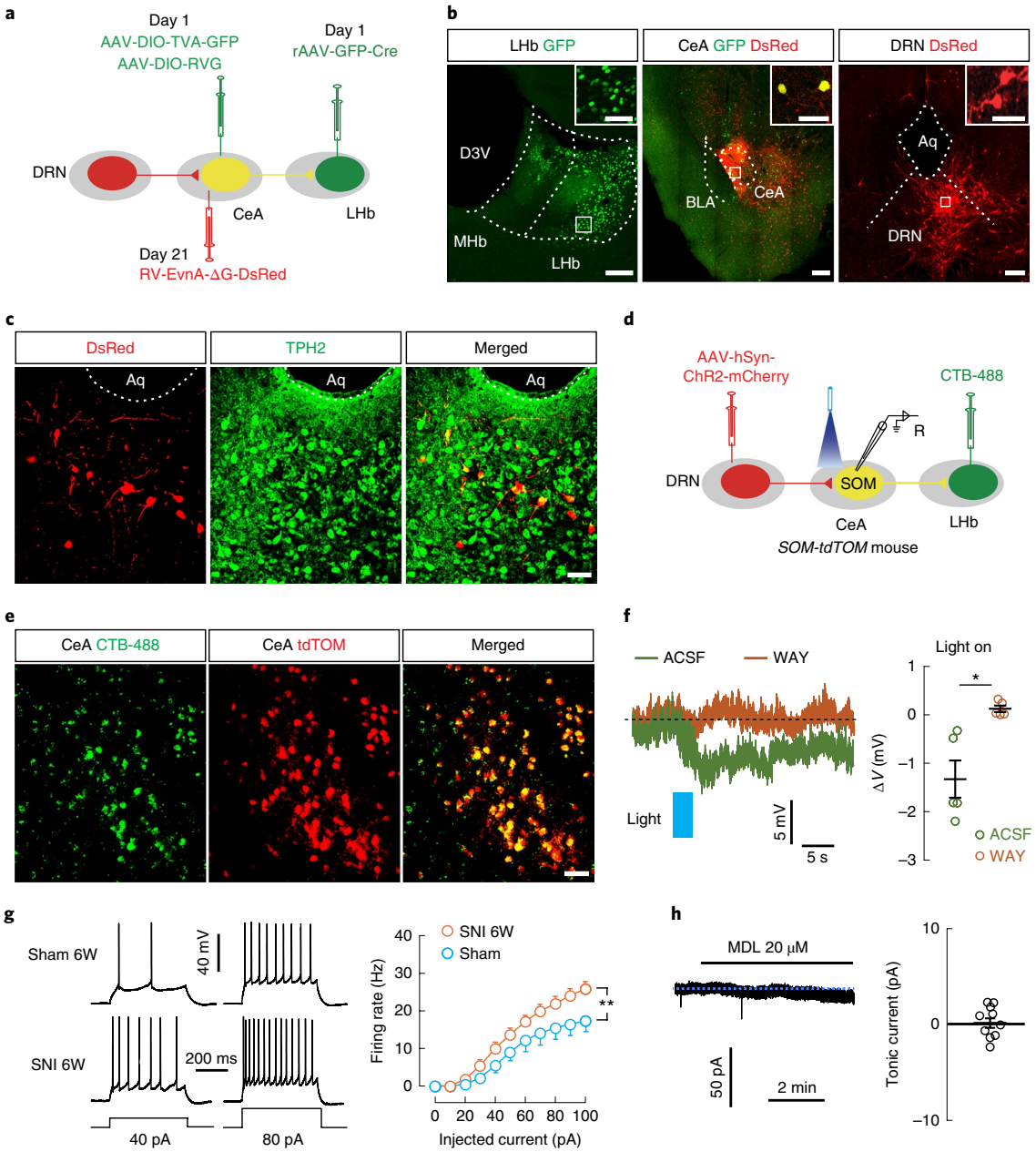

Fig. 6 | Dissection of the 5-HT^{DRN}→SOM^{CeA}→Glu^{LHb} circuit. a–c, Schematic of viral injection for triple retrograde tracing (**a**) and representative images of viral expression in the indicated nuclei (**b**). DsRed signals from the CeA were co-localized with TPH2 immunofluorescence in the DRN (**c**). Scale bars, 100 μm in **b** and 50 μm in **c**. Aq, aqueduct. **d**, Schematic of viral and CTB-488 injection for recording configuration in acute slices from *SOM-tdTOM* mice treated with SNI 6W or Sham 6W. **e**, Representative images of CTB-488 expression in the CeA. The experiment was independently repeated with similar results in $n=5$ mice. Scale bar, 50 μm. **f**, Sample traces and summarized data showing hyperpolarized potentials recorded from SOM^{CeA} neurons that were evoked by optical activation of 5-HT^{DRN} terminals in the CeA with or without the application of WAY (yellow cells in **e**, $n=5$ cells, $t_4=3.61$, $P=0.0226$). **g**, Representative action potential traces (left) and summarized data (right) recorded from SOM^{CeA} neurons (yellow cells in **e**, sham 6W, $n=12$ cells; SNI 6W, $n=15$ cells; $F_{10,250}=4.091$, $P<0.0001$). **h**, Representative current traces (left) and summarized data (right) showing the effect of MDL on SOM^{CeA} neurons (yellow cells in **e**, $n=10$ cells recorded from four mice). Significance was assessed by a two-tailed paired Student's *t*-test in **f**, and two-way repeated measures ANOVA with post hoc comparison between groups in **g**. The data are presented as the mean ± s.e.m. $^*P<0.05$; $^{**}P<0.01$.

pathways may be involved in the mechanism by which the 5-HT^{DRN} maladaptation contributes to the enhancement of glutamatergic synaptic transmission; for example, from the lateral amygdala onto SOM$^+$ CeA neurons[20]. Because SOM$^+$ neuronal activity is tonically regulated by presynaptic serotonin, the maladaptation of the 5-HT^{DRN}→SOM^{CeA} circuit may be maintained stably in persistent pain states. This complex profile may underlie the treatment-resistant character of depression in patients with CDS.

The LHb receives projections from many brain regions involved in the stress response, which may mediate separate symptoms of depression[36,37]. Previous work has shown that synaptic activity of LHb glutamatergic neurons is enhanced in animal models of depression[35]. Our results showed that SOM^{CeA} neurons mainly innervate Glu^{LHb} neurons through glutamatergic projections, which is similar to the previous finding that ventral pallidum PV neurons transmit glutamatergic signals[36]. It is thus likely that, in mice with chronic

pain and depressive-like symptoms, Glu^{LHb} neuronal activity is excited by increased SOM^{CeA} glutamatergic inputs. This hypothesis supports the notion that enhanced synaptic efficacy of habenula neurons contributes to depression-like behavior in rodents[35]. We thus propose that, although the LHb is a common region involved in the pathophysiology of depression[36,37], alterations in the cell type-specific regulation of the tone of the $5\text{-}HT^{DRN}\rightarrow SOM^{CeA}$ circuit could be a general mechanism for the development of treatment-resistant depression, including CDS. In addition, although the $5\text{-}HT^{DRN}\rightarrow SOM^{CeA}$ circuit likely contributes to multiple behavioral outputs, such as fear, anxiety and depression[15], the specific projection of this circuit to the LHb could be relatively more important for chronic pain-related behavioral alterations in the mouse models used in this study. These findings raise the possibility that different etiologies of depression, for example, chronic pain and stress, may be encoded by distinct circuits.

We found that activating the $5\text{-}HT^{DRN}\rightarrow SOM^{CeA}$ circuit relieved painful symptoms. This effect could involve amygdala-mediated descending pain-control systems[10,11]. As pharmacological options for the treatment of CDS remain limited, these findings raise the possibility of developing treatments that involve the use of dual-acting drugs or non-drug approaches, such as deep brain stimulation or transcranial magnetic stimulation[46,47], to target the converging pathways.

Online content

Any methods, additional references, Nature Research reporting summaries, source data, statements of code and data availability and associated accession codes are available at https://doi.org/10.1038/s41593-019-0468-2.

Received: 17 January 2019; Accepted: 15 July 2019;
Published online: 26 August 2019

References

1. Bair, M. J., Robinson, R. L., Katon, W. & Kroenke, K. Depression and pain comorbidity: a literature review. *Arch. Intern. Med.* **163**, 2433–2445 (2003).
2. McWilliams, L. A., Goodwin, R. D. & Cox, B. J. Depression and anxiety associated with three pain conditions: results from a nationally representative sample. *Pain* **111**, 77–83 (2004).
3. Simon, G. E., VonKorff, M., Piccinelli, M., Fullerton, C. & Ormel, J. An international study of the relation between somatic symptoms and depression. *New Engl. J. Med.* **341**, 1329–1335 (1999).
4. Arnow, B. A. et al. Comorbid depression, chronic pain, and disability in primary care. *Psychosom. Med* **68**, 262–268 (2006).
5. Goyal, M. et al. Meditation programs for psychological stress and well-being: a systematic review and meta-analysis. *JAMA Intern. Med.* **174**, 357–368 (2014).
6. Turk, D. C. & Gatchel, R. J. *Psychological Approaches to Pain Management: A Practitioner's Handbook* (Guilford Publications, 2018).
7. Campbell, L. C., Clauw, D. J. & Keefe, F. J. Persistent pain and depression: a biopsychosocial perspective. *Biol. Psychiatry* **54**, 399–409 (2003).
8. Strigo, I. A., Simmons, A. N., Matthews, S. C., Arthur, D. & Paulus, M. P. Association of major depressive disorder with altered functional brain response during anticipation and processing of heat pain. *Arch. Gen. Psychiatry* **65**, 1275–1284 (2008).
9. Martin, S. L. et al. 5-HT modulation of pain perception in humans. *Psychopharmacology* **234**, 2929–2939 (2017).
10. Kuner, R. Central mechanisms of pathological pain. *Nat. Med.* **16**, 1258–1266 (2010).
11. Kim, Y. S. et al. Central terminal sensitization of TRPV1 by descending serotonergic facilitation modulates chronic pain. *Neuron* **81**, 873–887 (2014).
12. Lee, Y. C., Nassikas, N. J. & Clauw, D. J. The role of the central nervous system in the generation and maintenance of chronic pain in rheumatoid arthritis, osteoarthritis and fibromyalgia. *Arthritis Res. Ther.* **13**, 211 (2011).
13. Basbaum, A. I., Bautista, D. M., Scherrer, G. & Julius, D. Cellular and molecular mechanisms of pain. *Cell* **139**, 267–284 (2009).
14. Bushnell, M. C., Ceko, M. & Low, L. A. Cognitive and emotional control of pain and its disruption in chronic pain. *Nat. Rev. Neurosci.* **14**, 502–511 (2013).
15. Ren, J. et al. Anatomically defined and functionally distinct dorsal raphe serotonin sub-systems. *Cell* **175**, 472–487 (2018).
16. Commons, K. G. Ascending serotonin neuron diversity under two umbrellas. *Brain Struct. Funct.* **221**, 3347–3360 (2016).
17. Hamilton, J. P., Siemer, M. & Gotlib, I. H. Amygdala volume in major depressive disorder: a meta-analysis of magnetic resonance imaging studies. *Mol. Psychiatry* **13**, 993–1000 (2008).
18. Amat, J. et al. Medial prefrontal cortex determines how stressor controllability affects behavior and dorsal raphe nucleus. *Nat. Neurosci.* **8**, 365 (2005).
19. Tye, K. M. et al. Amygdala circuitry mediating reversible and bidirectional control of anxiety. *Nature* **471**, 358–362 (2011).
20. Li, H. et al. Experience-dependent modification of a central amygdala fear circuit. *Nat. Neurosci.* **16**, 332–339 (2013).
21. Neugebauer, V., Li, W., Bird, G. C. & Han, J. S. The amygdala and persistent pain. *Neuroscientist* **10**, 221–234 (2004).
22. Han, S., Soleiman, M. T., Soden, M. E., Zweifel, L. S. & Palmiter, R. D. Elucidating an affective pain circuit that creates a threat memory. *Cell* **162**, 363–374 (2015).
23. Penzo, M. A. et al. The paraventricular thalamus controls a central amygdala fear circuit. *Nature* **519**, 455–459 (2015).
24. Haubensak, W. et al. Genetic dissection of an amygdala microcircuit that gates conditioned fear. *Nature* **468**, 270–276 (2010).
25. Hieronymus, F., Lisinski, A., Nilsson, S. & Eriksson, E. Efficacy of selective serotonin reuptake inhibitors in the absence of side effects: a mega-analysis of citalopram and paroxetine in adult depression. *Mol. Psychiatry* **23**, 1731–1736 (2017).
26. Barbui, C., Furukawa, T. A. & Cipriani, A. Effectiveness of paroxetine in the treatment of acute major depression in adults: a systematic re-examination of published and unpublished data from randomized trials. *CMAJ* **178**, 296–305 (2008).
27. Gonchar, Y., Wang, Q. & Burkhalter, A. Multiple distinct subtypes of GABAergic neurons in mouse visual cortex identified by triple immunostaining. *Front Neuroanat.* **1**, 3 (2007).
28. Scott, M. M. et al. A genetic approach to access serotonin neurons for in vivo and in vitro studies. *Proc. Natl Acad. Sci. USA* **102**, 16472–16477 (2005).
29. Madisen, L. et al. A robust and high-throughput Cre reporting and characterization system for the whole mouse brain. *Nat. Neurosci.* **13**, 133–140 (2010).
30. Marcinkiewcz, C. A. et al. Serotonin engages an anxiety and fear-promoting circuit in the extended amygdala. *Nature* **537**, 97–101 (2016).
31. Mogil, J. S. Animal models of pain: progress and challenges. *Nat. Rev. Neurosci.* **10**, 283–294 (2009).
32. Dworkin, R. H. et al. Pharmacologic management of neuropathic pain: evidence-based recommendations. *Pain* **132**, 237–251 (2007).
33. Decosterd, I. & Woolf, C. J. Spared nerve injury: an animal model of persistent peripheral neuropathic pain. *Pain* **87**, 149–158 (2000).
34. Shabel, S. J., Proulx, C. D., Piriz, J. & Malinow, R. Mood regulation. GABA/glutamate co-release controls habenula output and is modified by antidepressant treatment. *Science* **345**, 1494–1498 (2014).
35. Li, B. et al. Synaptic potentiation onto habenula neurons in the learned helplessness model of depression. *Nature* **470**, 535–539 (2011).
36. Knowland, D. et al. Distinct ventral pallidal neural populations mediate separate symptoms of depression. *Cell* **170**, 284–297 e218 (2017).
37. Hikosaka, O. The habenula: from stress evasion to value-based decision-making. *Nat. Rev. Neurosci.* **11**, 503–513 (2010).
38. Tervo, D. G. et al. A designer AAV variant permits efficient retrograde access to projection neurons. *Neuron* **92**, 372–382 (2016).
39. Bzdok, D., Laird, A. R., Zilles, K., Fox, P. T. & Eickhoff, S. B. An investigation of the structural, connectional, and functional subspecialization in the human amygdala. *Hum. Brain Mapp.* **34**, 3247–3266 (2013).
40. Amunts, K. et al. Cytoarchitectonic mapping of the human amygdala, hippocampal region and entorhinal cortex: intersubject variability and probability maps. *Anat. Embryol.* **210**, 343–352 (2005).
41. Ehnvall, A., Mitchell, P. B., Hadzi-Pavlovic, D., Malhi, G. S. & Parker, G. Pain during depression and relationship to rejection sensitivity. *Acta Psychiatr. Scand.* **119**, 375–382 (2009).
42. Howland, R. H. et al. Factors predicting reduced antidepressant response: experience with the SNRI duloxetine in patients with major depression. *Ann. Clin. Psychiatry* **20**, 209–218 (2008).
43. Cortes-Altamirano, J. L. et al. Review: 5-Ht1, 5-Ht2, 5-Ht3, And 5-Ht7 receptors and their role in the modulation of pain response in the central nervous system. *Curr. Neuropharmacol.* **16**, 210–221 (2018).
44. Savitz, J., Lucki, I. & Drevets, W. C. 5-HT1A receptor function in major depressive disorder. *Prog. Neurobiol.* **88**, 17–31 (2009).
45. Asmundson, G. J. & Katz, J. Understanding the co-occurrence of anxiety disorders and chronic pain: state-of-the-art. *Depress. Anxiety* **26**, 888–901 (2009).
46. Pascual-Leone, A., Rubio, B., Pallardo, F. & Catala, M. D. Rapid-rate transcranial magnetic stimulation of left dorsolateral prefrontal cortex in drug-resistant depression. *Lancet* **348**, 233–237 (1996).
47. Taghva, A. S., Malone, D. A. & Rezai, A. R. Deep brain stimulation for treatment-resistant depression. *World Neurosurg.* **80**, S27 e17–24 (2013).

Acknowledgements

We thank X. Yu and Y. Yang for providing Ai9 (RCL-tdT) mice. We thank F. Xu and T. Xue for technical support. All data are available in the main text or the Supplementary Data. Support for this study was provided by the National Natural Science Foundation of China (grant nos. 81870877, 91732303 and 91849119 to Z.Z.); the National Key Research and Development Program of China (grant no. 2016YFC1305900 to Z.Z.); the Strategic Priority Research Program of the Chinese Academy of Sciences (grant no. XDB02010000 to Z.Z.) and the National Natural Science Foundation of China (grant no. 31600851 to W.T. and grant no. 81600964 to Y.J.).

Author contributions

W.Z., Y.J., Q.M. and X.Zhu designed the studies, performed most of the experiments and data analysis, and wrote the draft manuscript. T.B., Y.T., Y.M., L.W., H.Z., B.-S.Q., X.Zhang, Y.L. and W.X. conducted the fMRI experiments and data analyses and wrote the text of the final manuscript. W.T., H.W., Jie Li and N.Z. conducted some of the molecular and behavioral experiments. X.L., M.-H.L., Juan Li and H.X. designed the viral tracing experiments in *CR-Cre*, *PV-Ce* and *SOM-Cre* mice. Patients with chronic pain or depression were evaluated by certified doctors Y.M., Y.T., W.X. and K.W. J.Z., K.W., G.R.L., L.X. and Z.Z. were involved in the overall design of the study and the revision of the final manuscript. Z.Z. was involved in the overall design of the project, individual experiments, data analysis and the writing of the final manuscript.

Competing interests

The authors declare no competing interests.

Additional information

Supplementary information is available for this paper at https://doi.org/10.1038/s41593-019-0468-2.

Reprints and permissions information is available at www.nature.com/reprints.

Correspondence and requests for materials should be addressed to Z.Z.

Peer review information: *Nature Neuroscience* thanks Rohini Kuner, Manuel Mameli and the other, anonymous, reviewer(s) for their contribution to the peer review of this work.

Publisher's note: Springer Nature remains neutral with regard to jurisdictional claims in published maps and institutional affiliations.

© The Author(s), under exclusive licence to Springer Nature America, Inc. 2019

Methods

Animals. In all experiments, C57BL/6J, *GAD2-Cre*, *CaMKII-Cre*, *SOM-Cre*, *CR-Cre*, *PV-Cre*, *Pet1-Cre* and *Ai9* (RCL-tdT) male mice (purchased from Charles River or Jackson Laboratories) at 8–10 weeks of age were used. Until the cannula surgery, the mice were housed five per cage in a colony with ad libitum access to water and food (standard mouse chow). They were maintained under a 12-h light/dark cycle (lights on from 07:00 to 19:00) at a stable temperature (23–25 °C). Mice were randomly assigned to experimental groups. All animal protocols were approved by the Animal Care and Use Committee of the University of Science and Technology of China.

Animal models of inflammatory pain. CFA (10 µl, Sigma-Aldrich) was injected into the plantar surface of the left hind paws of mice using an insulin syringe (BD Corporation) under brief isoflurane anesthesia to induce persistent inflammatory pain. The persistence of inflammatory pain was ensured by a second CFA (10 µl) injection on the tenth day. Saline (0.9% NaCl) was injected as control.

Animal models of neuropathic pain. The SNI surgery was performed under anesthesia with isoflurane. The skin and muscle of the left thigh were incised to explore the sciatic nerve consisting of the sural, common peroneal and tibial nerves. After exploration, nonabsorbent 5.0 chromic gut sutures were used to ligate the common peroneal and tibial nerves, and then the nerves were transected and about 2 mm sections from the dot were removed. The skin was stitched and disinfected with iodophor. For the sham mice, the procedure was the same as for the experimental group except that the nerves were left intact. The mechanical pain threshold was assessed by von Frey filaments.

Virus injection. Before surgery, the mice were fixed in a stereotactic frame (RWD) under a combination of xylazine (10 mg kg^{-1}) anesthesia and ketamine (100 mg kg^{-1}) analgesia. A heating pad was used to maintain the core body temperature of the animals at 36 °C. A volume of 100–300 nl virus (depending on the expression strength and viral titer) was injected using calibrated glass microelectrodes connected to an infusion pump (micro 4, WPI) at a rate of 30 nl min^{-1}. The coordinates were defined as dorso-ventral (DV) from the brain surface, anterior--posterior (AP) from bregma and medio-lateral (ML) from the midline (in mm).

For retrograde monosynaptic tracing, helper viruses that contained rAAV-Ef1α-DIO-RVG-WPRE-pA (AAV-DIO-RVG, AAV2/9, 2×10^{12} viral genome (vg) ml^{-1}) and rAAV-Ef1α-DIO-EGFP-2a-TVA-WPRE-pA (AAV-DIO-TVA-GFP, AAV2/9, 2×10^{12} vg ml^{-1}; 1:2, 200 nl) were co-injected into the right CeA of *Cre* transgenic mice[48] (AP, −1.18 mm; ML, −2.65 mm; DV, −4.25 mm). After 3 weeks, the rabies virus RV-ENVA-ΔG-DsRed (2×10^{8} integral field units per ml, 300 nl) was injected into the same site in the CeA. The modified rabies virus cannot infect neurons and spread retrogradely without the TVA and rabies glycoprotein component, which is provided by AAV helpers[49]. For 5-HT^{DRN}→SOM^{CeA}→LHb triple tracing, the AAV$_{2/2}$Retro-CMV-bGl-Cre-EGFP virus (AAV-CRE-GFP, 1.83×10^{13} vg ml^{-1}, 100 nl; Taitool) was first injected into the right LHb (AP, −1.95 mm; ML, −0.35 mm; DV, −2.65 mm) to allow the virus spread retrogradely to CeA soma to express Cre-GFP; simultaneously, the Cre-dependent mixed helper virus was infused into the ipsilateral CeA. The rabies virus was injected after 3 weeks. Mice that had been anesthetized with pentobarbital (20 mg kg^{-1}, i.p.) were transcardially perfused 7 d after the last injection and brain slices were prepared (40 µm) for tracing DsRed or co-staining with TPH2 antibody. The retrograde tracer CTB-488 (0.1% mg ml^{-1}, 100 nl, Thermolife) was injected into the CeA of *Pet1-tdTOM* mice for 5 d to label CeA-projecting 5-HT^{DRN} neurons or the LHb of *SOM-tdTOM* mice to label LHb-projecting SOM^{CeA} neurons for visualized electrophysiological recordings.

For anterograde tracing, the Cre-dependent virus rAAV-Ef1α-DIO-hChR2 (H134R)-mCherry-WPRE-pA (AAV-DIO-ChR2-mCherry, AAV2/9, 1.63×10^{13} vg ml^{-1}, 200 nl) was delivered into the DRN of *Pet1-Cre* mice (AP, −4.65 mm; ML, 0 mm; DV, −2.85 mm) or the CeA of *SOM-Cre* mice. After 4 weeks, the expression of mCherry was detected in the whole brain and optogenetic manipulation was performed. In some experiments, rAAV-hSyn-hChR2-EYFP-WPRE-pA (AAV-hSyn-ChR2-EYFP, AAV2/9, 2.09×10^{12} vg ml^{-1}: enhanced yellow fluorescent protein), rAAV-hSyn-hChR2-mCherry-WPRE-pA (AAV-hSyn-ChR2-mCherry, AAV2/9, 3.06×10^{12} vg ml^{-1}) or rAAV-Ef1α-DIO-eNpHR3.0-EYFP-WPRE-pA (AAV2/9, 1.18×10^{13} vg ml^{-1}) were used for optogenetic manipulation. The rAAV-Ef1α-DIO-hM3D(Gq)-mCherry-WPRE-pA (AAV-DIO-hM3Dq-mCherry, AV2/8, 2.69×10^{13} vg ml^{-1}) and rAAV-Ef1α-DIO-hM4D(Gi)-mCherry-WPRE-pA (AAV-DIO-hM4Di-mCherry, AAV2/9, 3.69×10^{13} vg ml^{-1}) viruses were used for chemogenetic manipulations 3 weeks after injection. The rAAV-Ef1α-DIO-mCherry-WPRE-pA (AAV2/8, 8.93×10^{12} vg ml^{-1}) and rAAV-DIO-EYFP-WPRE-pA (AAV2/9, 1.95×10^{12} vg ml^{-1}) viruses were used as the controls. For the anterograde tracing of the CeA-LHb circuit, we injected AAV2/1-hSyn-Cre (1.23×10^{13} vg ml^{-1}, 100 nl; Taitool) into the CeA, which enabled the Cre enzyme to spread anterogradely and monosynaptically into the soma of LHb neurons. Then, Cre-dependent AAV-DIO-GFP was injected into the ipsilateral LHb. Three weeks later, the mice were perfused and the brain were sliced for imaging. Unless otherwise stated, all viruses were packaged by BrainVTA. All mice were transcardially perfused with 0.9% saline followed by ice-cold phosphate buffer (0.1 M) that contained 4% paraformaldehyde. Images of the signal expression were acquired with a confocal microscope (LSM 710, ZEISS). Animals with missed injections were excluded.

Optogenetic manipulations in vivo. An optical fiber was initially implanted into the right CeA and LHb in the brain of an anesthetized mouse that had been immobilized in a stereotaxic apparatus. The implant fiber was secured to the animal's skull with dental cement. Chronically implantable fibers (diameter, 200 µm, Newdoon) were connected to a laser generator using optic fiber sleeves. The delivery of a 5-min pulse of blue light (473 nm, 1–3 mW, 15 ms pulses, 20 Hz) or yellow light (594 nm, 5–8 mW, constant) was controlled by a Master-8 pulse stimulator (A.M.P.I.). The same stimulus protocol was applied in the control group. The location of the fibers was examined after all the experiments, and data obtained from mice in which the fibers were outside the desired brain region were discarded. Behavioral assays were performed immediately after light stimulation.

Local drug infusion. An internal stainless-steel injector attached to a 10 µl syringe (Hamilton) and an infusion pump was inserted into the guide cannula (internal diameter 0.34 mm, RWD) and used to infuse WAY100635 (0.25 nM in 200 nl) into the right CeA at a flow rate of 100 nl min^{-1}. Similarly, paroxetine (0.5 µM in 200 nl), 8-OH (3.2 nM in 200 nl) or vehicle solution (ACSF, 200 nl) was locally applied. The injector was slowly withdrawn 2 min after the infusion and the behavioral assays were performed roughly 30 min after the infusion. The mice were allowed at least 10 d for recovery before injections to minimize stress during the behavioral assays, and the mice with missed injections were excluded from the study.

Unless otherwise stated, all drugs were purchased from Sigma-Aldrich. Tetrodotoxin was obtained from Hebei Aquatic Science and Technology Development Company. Paroxetine, WAY100635 and MDL100907 were obtained from Tocris.

Brain slice electrophysiology. *Brain slice preparation.* Mice were deeply anesthetized with pentobarbital sodium (2% w/v, i.p.) and intracardially perfused with ~20 ml ice-cold oxygenated modified NMDG artificial cerebrospinal fluid (NMDG ACSF) that contained (in mM) 93 *N*-methyl-D-glucamine (NMDG), 2.5 KCl, 1.2 NaH_2PO_4, 30 $NaHCO_3$, 20 HEPES, 25 glucose, 2 thiourea, 5 Na-ascorbate, 3 Na-pyruvate, 0.5 $CaCl_2$, 10 $MgSO_4$ and 3 glutathione (GSH). The pH of the ACSF was 7.3–7.4 and osmolarity was 300–305 mOsm kg^{-1}. Coronal slices (300 µm) that contained the DRN, CeA or LHb were sectioned at 0.18 mm s^{-1} on a vibrating microtome (VT1200s, Leica). The brain slices were initially incubated in NMDG ACSF for 10–12 min at 33 °C, followed by *N*-2-hydroxyethylpiperazine-*N*-2-ethanesulfonic acid (HEPES) ACSF that contained (in mM) 92 NaCl, 2.5 KCl, 1.2 NaH_2PO_4, 30 $NaHCO_3$, 20 HEPES, 25 glucose, 2 thiourea, 5 Na-ascorbate, 3 Na-pyruvate, 2 $CaCl_2$, 2 $MgSO_4$ and 3 GSH (pH 7.3–7.4, osmolarity 300–305 mOsm kg^{-1}) for at least 1 h at 25 °C. The brain slices were transferred to a slice chamber (Warner Instruments) for electrophysiological recording and were continuously perfused with standard ACSF that contained (in mM) 129 NaCl, 2.4 $CaCl_2$, 3 KCl, 1.3 $MgSO_4$, 20 $NaHCO_3$, 1.2 KH_2PO_4 and 10 glucose (pH 7.3–7.4, osmolarity 300–305 mOsm kg^{-1}) at 2.5–3 ml min^{-1} at 32 °C. The temperature of the ACSF was maintained by an in-line solution heater (TC-344B, Warner Instruments). The recorders were blinded to the group identity during recording and analyses.

Whole-cell patch-clamp recordings. Neurons in the slice were visualized using a ×40 water-immersion objective on an upright microscope (BX51WI, Olympus) equipped with infrared-differential interference contrast (IR-DIC) and an infrared camera connected to the video monitor. Whole-cell patch-clamp recordings were obtained from visually identified DRN, CeA or LHb cells. Patch pipettes (3–5 MΩ) were pulled from borosilicate glass capillaries (VitalSense Scientific Instruments Co., Ltd) with an outer diameter of 1.5 mm on a four-stage horizontal puller (P1000, Sutter Instruments). The signals were acquired via a Multiclamp 700B amplifier, low-pass filtered at 2.8 kHz, digitized at 10 kHz and analyzed with Clampfit 10.7 software (Molecular Devices). If the series resistance changed more than 20% during the recording, the experimental recording was immediately terminated.

Synaptic transmission. Neurons were held at −70 mV using the voltage clamp mode for recording mIPSCs, as performed in our previous study[50]. The pipettes were filled with intracellular solution that contained (in mM) 145 CsCl, 10 EGTA, 10 HEPES, 2 $MgCl_2$, 2 $CaCl_2$, 2 Mg-ATP and 5 QX-314. The osmolarity of the solution was adjusted to 285–290 mOsm kg^{-1} and the pH was adjusted to 7.2 with KOH. Then, 6,7-dinitroquinoxaline-2,3(1*H*,4*H*)-dione (10 µM) was added to eliminate excitatory components and 1 µM tetrodotoxin was added to the bath solution to eliminate spontaneous action potentials. The baseline was recorded for at least 5 min before the application of 5-HT (25 µM). In a subset of experiments, MDL100907 (20 µM) was added to the standard ACSF and the slices were incubated in this drug solution for at least 10 min before the experiments. The current-evoked firing was recorded in current-clamp mode (I = 0 pA). The threshold current for firing was defined as the minimum strength of current injection required to elicit at least one or two spikes.

Light-evoked responses. Optical stimulation was delivered using a laser (Shanghai Fiblaser Technology Co., Ltd) through an optical fiber 200 µm in diameter positioned 0.2 mm from the surface of the brain slice. To test the functional characteristics of AAV-DIO-ChR2, fluorescently labeled neurons that expressed ChR2 in *Pet1-Cre*, *GAD2-Cre* or *SOM-Cre* mice 3–4 weeks after virus injection were visualized and stimulated with a blue (473 nm, 5–10 mV) laser light using 5, 10 or 20 Hz stimulation protocols with a pulse width of 15 ms. In some experiments, the function of eNpHR3.0 was assessed by applying sustained yellow (594 nm, 1–5 mV, 200 ms) laser light stimulation. To assess the function of 5-HT fibers from the DRN that express ChR2, sustained photostimulation (473 nm, 3 s, 20 Hz, 15 ms) was delivered to CeA retrograde tracer-positive SOM^+ neurons from *Pet1-Cre* or *SOM-tdTOM* mice in which the LHb had been injected with the retrograde tracer CTB-488. For electrophysiological recording of CeA-LHb synaptic transmission, light (473 nm, 1 s, 10 Hz, 10 ms) was delivered to the LHb of *SOM-Cre* mice in which the CeA had been injected with AAV-DIO-ChR2-mCherry and the internal solution containing (in mM): 130 Cs-methanesulfonate, 2 $MgCl_2$, 2 $CaCl_2$, 10 EGTA, 10 HEPES, 2 Mg-ATP and 5 QX-314 was used. The picrotoxin and α-amino-3-hydroxy-5-methyl-4-isoxazolepropionic acid receptor antagonist 6,7-dinitroquinoxaline-2,3(1*H*,4*H*)-dione were added to block the excitatory and inhibitory effects.

Immunohistochemistry. The mice were deeply anesthetized with pentobarbital sodium (50 mg kg^{-1}, i.p.) and sequentially perfused with saline and 4% (w/v) paraformaldehyde. The brains were subsequently removed and post-fixed in 4% paraformaldehyde at 4 °C overnight. After cryoprotection of the brains with 30% (w/v) sucrose, coronal sections (40 µm) were cut on a cryostat (Leica CM1860) and used for immunofluorescence. The sections were incubated in 0.3% (v/v) Triton X-100 for 0.5 h, blocked with 10% donkey serum for 1 h at room temperature, and incubated with primary antibodies, including anti-TPH2 (1:500, goat, Abcam) anti-5-HT_{1A}Rs (1:200, rabbit, Abcam; 1:400, mouse, Sigma), anti-VGLUT2 (1:500, rabbit, Millipore), anti-SOM (1:50, goat, Santa Cruz), anti-c-Fos (1:500, rabbit, Santa Cruz) and anti-5-HT_{2A}Rs (1:200, rabbit, Abcam) at 4 °C for 24 h, followed by the corresponding fluorophore-conjugated secondary antibodies for 2 h at room temperature. For the c-Fos assay, the 5-HT^{DRN}-CeA circuit was optically inhibited for 10 min, and the mice were perfused 90 min later. Fluorescence signals were visualized using a Leica DM2500 camera and Zeiss LSM710 microscope.

Assessment of depressive-like behavior. For all behavioral tests, mice were transported in a holding cabinet to the testing room where they were habituated at least 1 d before testing. During the testing session, the behavior of the animals was recorded using a video tracking system and was subsequently analyzed offline. Dim light (~20 lux) was used in the room to minimize the anxiety of the animals. The experimenter was blinded to group identity during the experiment and quantitative analyses.

OFT. Mice were placed in one corner of an open field apparatus that consists a square area (25 × 25 cm^2) and a marginal area (50 × 50 × 60 cm^3); the mice were allowed to freely explore their surroundings. The animals' movement trajectories were recorded for 5 min using EthoVision XT software, which records the number of entries into and the amount of time spent in the central area. The area was cleaned with 75% ethanol after each test to remove olfactory cues from the apparatus.

EPM test. The EPM consists of a central platform (6 × 6 cm^2), two closed arms (30 × 6 × 20 cm^3) and two opposing open arms (30 × 6 cm^2). The maze was placed 100 cm above the floor, and the light levels in the open arms were ~20 lux. A mouse was placed in the central platform facing a closed arm and was allowed to explore the maze for 5 min. The time spent in the open arms and the number of entries into the open arms were analyzed using EthoVision XT software (Noldus). The area was cleaned between tests using 75% ethanol.

SPT. Mice were housed individually and habituated with two identical bottles of 1% sucrose for 2 d followed with 2 d of water. Then the experimental mice were water deprived for 24 h. Next, the mice were presented with two bottles for 2 h, one containing water and the other containing 1% sucrose, and the bottles' positions were switched after 1 h. The consumption of each fluid was measured. For the optogenetic experiment, the mice were subjected to light epochs of 30 min on/30 min off/30 min off/30 min off and the consumption of each fluid was measured.

TST. Mice were individually suspended about 50 cm above the surface of a table using adhesive tape that was placed roughly 1 cm from the tip of the tail. Each mouse was tested only once for 6 min; the test was videotaped from the side and the immobility time of the animal was measured in the last 5 min. Mice were considered immobile without initiated movements; immobility was considered to include passive swaying. For the optogenetic experiments, the mice were first suspended for 2 min and then subjected to light epochs of 3 min off/3 min on/3 min off.

Repeated. SDS. The aggressive retired male breeder CD1 mice were screened with male C57 mice for three consecutive days and housed individually. During the following 10 d, the experimental mice were placed in the home cage of the CD1 mice and allowed physical contact with them for 10 min every day. Then the mice were separated by transparent Plexiglas that allowed sensory contact for 24 h until the next bout of physical defeat with a new CD1 mouse. After 10 d of social defeat, the experimental mice were housed individually and their depression-like behavior was tested.

CRS. Mice were periodically constrained from moving by placing them in a 50-ml syringe for 6 h every day for 3 weeks. Holes were drilled in the ends of the syringes for mouse breathing. During the restraint period, the control mice were allowed to freely move in the cage without water or food provided. The syringes were thoroughly washed every day after the restraint. To exclude the effect of acute stress, the mice were allowed to rest 1 d after CRS before the anatomical and electrophysiological experiments were conducted.

In vivo microdialysis-HPLC. Electrochemical detection in combination with HPLC (ANTEC) was used to measure the 5-HT concentration in the CeAs of freely moving mice. A microdialysis probe (CMA7, CMA) connected to a syringe infusion pump (CMA402, CMA) via polyethylene tubing was initially implanted into the right CeA of deeply anesthetized mice. The tissue was perfused with normal Ringer's solution (3 mM KCl, 145 mM NaCl and 1.3 mM $CaCl_2$) via the pump at a rate of 0.25 µl min^{-1} and the dialysate was collected for 2 h through the probe in freely moving mice. The dialysate was loaded automatically to the mobile phase (50 mM phosphoric acid, 8 mM NaCl, 0.1 mM EDTA, 12.5% methanol and 500 mg l^{-1} octane sulfate, pH = 6.0) and separated in a 1 × 50 mm^2 column (ALF-105, ANTEC) with a 3 µm particle size at a rate of 75 µl min^{-1}. Detection was conducted using an Alexys online analysis system (ANTEC Leyden) that consisted of a DECADE II electrochemical detector and VT-3 electrochemical flow cells. The data were analyzed using Clarity software (ANTEC) based on standard samples.

fMRI. *Participants.* This study was approved by the ethics committee of the First Affiliated Hospital of Anhui Medical University and was conducted in agreement with the principles set out in the Declaration of Helsinki. All patients in this study were recruited from the First Affiliated Hospital of Anhui Medical University (Hefei). Patients were diagnosed with major depressive disorder according to the fifth edition of the Diagnostic and Statistical Manual of Mental Disorders (DSM-V). The depression score was evaluated by the 17-item Hamilton Depression Rating Scale (HAMD)[51]. 'Moderate' depressive patients were recruited. The symptoms or functional impairment of these patients were between those of 'mild' and 'severe' patients who were hospitalized. All chronic pain (>1 year) originated from the lower back, which was diagnosed according to the McGill pain questionnaire and the tenth revision of the International Classification of Diseases by certified doctors[52,53]. We also enrolled age- and gender-matched healthy controls who were recruited by advertisement. The exclusion criteria for all participants included a current or past history of alcohol or drug dependency, pregnancy, neurological disorders and any contraindications to fMRI scans. After participants were informed of the purpose of the study, they were required to provide written informed consent before screening.

Data acquisition and preprocessing. All participants underwent MRI scans at the First Affiliated Hospital of Anhui Medical University. A Signa HDxt 3.0T whole-body MRI scanner was used with a standard echo planar imaging sequence. Resting-state functional data were collected using the following parameters: repetition time/echo time ratio = 2,000/22.5 ms; flip angle, 30°; field of view, 220 × 220; matrix size, 64 × 64; 33 slices and thickness/gap ratio, 4.0/0.6 mm. The scanning duration was 8 min. The Data Processing Assistant for the Resting-State fMRI (DPARSF) toolkit was used for image preprocessing. The first ten volumes were discarded to exclude the influence of unstable longitudinal magnetization and the remaining volumes were processed using the following steps: slice timing correction, realignment, normalization using echoplanar imaging (EPI) templates resampled at a resolution of 3 × 3 × 3 mm^3, spatial smoothing (4 mm full width at half maximum) and linear detrending. The data were also temporally bandpass-filtered (0.01–0.1 Hz) to limit low-frequency fluctuations and high-frequency noise. The global signal, the average signal across all voxels in the brain, is assumed to reflect a combination of resting-state fluctuations, physiological noise (for example, respiratory and cardiac noise) and other noise signals with non-neural origin, which could contaminate reported results[54,55]. Thus, we defined the white matter signal, the cerebrospinal fluid signal, the global signal and 24 Friston motion parameters as nuisance regressors to control for non-neuronal activation. No participants with excessive motion during scanning (>3 mm in translation or 3° in rotation) were included. For head motion indexed by the framewise displacement[56], no significant difference was observed between groups, nor was any significant difference observed after regressing out head motion. To ensure that the functional connectivity was not contaminated with motion, unpaired Student's *t*-test were conducted with the head motion parameters as covariates. A total of 105 participants were enrolled in the final analysis: 22 patients with chronic pain and depression, 29 patients with chronic pain but without depression, 27 depressed patients with no chronic pain and 27 healthy control participants.

Resting-state functional connectivity (rsFC) and statistical analysis. A seed-based correlation approach was used to analyze the resting-state functional connectivity. We created the right amygdala and bilateral CM seeds according to previous reports[39,40]. The detailed region masks are available at http://anima.fz-juelich.de/. Then, we computed Pearson's correlations between the time series of these nuclei and each voxel in the rest of the whole brain within each individual. Fisher's *z*-transformation was subsequently applied to improve the normality, and the results were displayed as rsFC maps for each individual. We further used an unpaired Student's *t*-test based on the rsFC map to determine areas that showed significantly different functional connectivity to the seed in different groups. All statistical maps were thresholded using the Monte Carlo simulation correction (corrected with $P<0.05$ for each voxel and a cluster volume >85 voxels). The Resting-State fMRI Data Analysis Toolkit (http://www.restfmri.net) was used to perform statistical analysis and present the surviving regions. Experimenters were blinded during the experiment and quantitative analysis was conducted to avoid biases. Although all experimental procedures and data analyses were performed as strictly as possible, some factors may confound the findings in fMRI studies, such as motion artifacts and antidepressants or analgesics that patients received.

Statistical analysis. We conducted simple statistical comparisons using Student's *t*-test. Analysis of variance (ANOVA) (one-and two-way) and post hoc analyses were used to statistically analyze the data from the experimental groups with multiple comparisons. No statistical methods were used to predetermine sample sizes, but our sample sizes were similar to those reported in previous publications[19,20,23]. Data distribution was assumed to be normal, but this was not formally tested. All data are expressed as the mean ± s.e.m., and significance levels are indicated as $^{*}P<0.05$, $^{**}P<0.01$ and $^{***}P<0.001$. OriginPro 2017 software (Origin Lab Corporation) and GraphPad Prism 5 (Graph Pad Software, Inc.) were used for the statistical analyses and graphing. Offline analysis of the data obtained from electrophysiological recordings was conducted using Clampfit software v.10.7 (Axon Instruments, Inc.) and MiniAnalysis software v.6.03 (Synaptosoft Inc.).

Reporting Summary. Further information on research design is available in the Nature Research Reporting Summary linked to this article.

Data availability

The data that support the findings of this study are available from the corresponding author upon request.

References

48. Wickersham, I. R. et al. Monosynaptic restriction of transsynaptic tracing from single, genetically targeted neurons. *Neuron* **53**, 639–647 (2007).
49. Wall, N. R., Wickersham, I. R., Cetin, A., De La Parra, M. & Callaway, E. M. Monosynaptic circuit tracing in vivo through Cre-dependent targeting and complementation of modified rabies virus. *Proc. Natl Acad. Sci. USA* **107**, 21848–21853 (2010).
50. Zhang, Z., Cai, Y.-Q., Zou, F., Bie, B. & Pan, Z. Z. Epigenetic suppression of GAD65 expression mediates persistent pain. *Nat. Med.* **17**, 1448 (2011).
51. Hamilton, M. A rating scale for depression. *J. Neurol. Neurosurg. Psychiatry* **23**, 56–62 (1960).
52. Melzack, R. The short-form McGill pain questionnaire. *Pain* **30**, 191–197 (1987).
53. Treede, R.-D. et al. A classification of chronic pain for ICD-11. *Pain* **156**, 1003 (2015).
54. Murphy, K., Birn, R. M., Handwerker, D. A., Jones, T. B. & Bandettini, P. A. The impact of global signal regression on resting state correlations: are anti-correlated networks introduced? *Neuroimage* **44**, 893–905 (2009).
55. Saad, Z. S. et al. Trouble at rest: how correlation patterns and group differences become distorted after global signal regression. *Brain Connect.* **2**, 25–32 (2012).
56. Jenkinson, M., Bannister, P., Brady, M. & Smith, S. Improved optimization for the robust and accurate linear registration and motion correction of brain images. *Neuroimage* **17**, 825–841 (2002).

nature research

Corresponding author(s): Zhi Zhang

Last updated by author(s): Jul 10, 2019

Reporting Summary

Nature Research wishes to improve the reproducibility of the work that we publish. This form provides structure for consistency and transparency in reporting. For further information on Nature Research policies, see Authors & Referees and the Editorial Policy Checklist.

Statistics

For all statistical analyses, confirm that the following items are present in the figure legend, table legend, main text, or Methods section.

n/a	Confirmed	
☐	☒	The exact sample size (*n*) for each experimental group/condition, given as a discrete number and unit of measurement
☐	☒	A statement on whether measurements were taken from distinct samples or whether the same sample was measured repeatedly
☐	☒	The statistical test(s) used AND whether they are one- or two-sided *Only common tests should be described solely by name; describe more complex techniques in the Methods section.*
☒	☐	A description of all covariates tested
☐	☒	A description of any assumptions or corrections, such as tests of normality and adjustment for multiple comparisons
☐	☒	A full description of the statistical parameters including central tendency (e.g. means) or other basic estimates (e.g. regression coefficient) AND variation (e.g. standard deviation) or associated estimates of uncertainty (e.g. confidence intervals)
☐	☒	For null hypothesis testing, the test statistic (e.g. *F*, *t*, *r*) with confidence intervals, effect sizes, degrees of freedom and *P* value noted *Give P values as exact values whenever suitable.*
☒	☐	For Bayesian analysis, information on the choice of priors and Markov chain Monte Carlo settings
☒	☐	For hierarchical and complex designs, identification of the appropriate level for tests and full reporting of outcomes
☐	☒	Estimates of effect sizes (e.g. Cohen's *d*, Pearson's *r*), indicating how they were calculated

Our web collection on statistics for biologists contains articles on many of the points above.

Software and code

Policy information about availability of computer code

Data collection	For slice physiological recording, the current and voltage signals were recorded with MultiClamp 700B and Clampex 10 data acquisition software (Molecular Devices, USA). For In vivo microdialysis-HPLC, the samples were collected microdialysis probe (CMA7, CMA, USA) and data were analyzed using Clarity software (ANTEC, Netherlands). Images were captured on a Zeiss LSM710 confocal microscope (Germany) or Leica DM2500 (Germany).A Signa HDxt 3.0 T whole-body MRI scanner was used for fMRI data acquisition. The Data Processing Assistant for Resting-State fMRI (DPARSF) toolkit was used for fMRI image preprocessing.
Data analysis	For slice physiological recording, the data was analyzed using Clampfit 10.3 (Molecular devices, USA) and MiniAnalysis software version 6.03 (Synaptosoft Inc., USA). Behavioral videos analyzed using EthoVision XT software (Noldus). OriginPro 2017 software (Origin Lab Corporation, USA) and GraphPad Prism 5 (Graph Pad Software, Inc., USA) were used for the statistical analyses. The Resting-State fMRI Data Analysis Toolkit (REST; http://www.restfmri.net) was used to perform statistical analysis and present the surviving regions.

For manuscripts utilizing custom algorithms or software that are central to the research but not yet described in published literature, software must be made available to editors/reviewers. We strongly encourage code deposition in a community repository (e.g. GitHub). See the Nature Research guidelines for submitting code & software for further information.

Data

Policy information about availability of data

All manuscripts must include a data availability statement. This statement should provide the following information, where applicable:

- Accession codes, unique identifiers, or web links for publicly available datasets
- A list of figures that have associated raw data
- A description of any restrictions on data availability

The data that support the findings of this study are available from the corresponding authors upon reasonable request.

Field-specific reporting

Please select the one below that is the best fit for your research. If you are not sure, read the appropriate sections before making your selection.

☒ Life sciences ☐ Behavioural & social sciences ☐ Ecological, evolutionary & environmental sciences

For a reference copy of the document with all sections, see nature.com/documents/nr-reporting-summary-flat.pdf

Life sciences study design

All studies must disclose on these points even when the disclosure is negative.

Sample size	No statistical methods were used to pre-determine sample sizes but our sample sizes are similar to those reported in previous publications (PMID: 21389985; PMID: 23354330;PMID: 25600269).
Data exclusions	For all experiments, mice with signs of infection/bleeding/unhealthy conditions after the surgeries were excluded for behavioral tests and mice with missed viral injections or implantation targets, as described by brain atlas, were not included in experimental analyses.
Replication	Behavioral experiments are replicated multiples times with independent mice, and at least two people independently analyzed time points for the behavioral events. Numbers of replicates (n) are indicated in the figure legends.
Randomization	The animals in the behavioral tests were randomized assigned.
Blinding	All investigators were blinded to group allocation during data collection and analysis.

Behavioural & social sciences study design

All studies must disclose on these points even when the disclosure is negative.

Study description	*Briefly describe the study type including whether data are quantitative, qualitative, or mixed-methods (e.g. qualitative cross-sectional, quantitative experimental, mixed-methods case study).*
Research sample	*State the research sample (e.g. Harvard university undergraduates, villagers in rural India) and provide relevant demographic information (e.g. age, sex) and indicate whether the sample is representative. Provide a rationale for the study sample chosen. For studies involving existing datasets, please describe the dataset and source.*
Sampling strategy	*Describe the sampling procedure (e.g. random, snowball, stratified, convenience). Describe the statistical methods that were used to predetermine sample size OR if no sample-size calculation was performed, describe how sample sizes were chosen and provide a rationale for why these sample sizes are sufficient. For qualitative data, please indicate whether data saturation was considered, and what criteria were used to decide that no further sampling was needed.*
Data collection	*Provide details about the data collection procedure, including the instruments or devices used to record the data (e.g. pen and paper, computer, eye tracker, video or audio equipment) whether anyone was present besides the participant(s) and the researcher, and whether the researcher was blind to experimental condition and/or the study hypothesis during data collection.*
Timing	*Indicate the start and stop dates of data collection. If there is a gap between collection periods, state the dates for each sample cohort.*
Data exclusions	*If no data were excluded from the analyses, state so OR if data were excluded, provide the exact number of exclusions and the rationale behind them, indicating whether exclusion criteria were pre-established.*
Non-participation	*State how many participants dropped out/declined participation and the reason(s) given OR provide response rate OR state that no participants dropped out/declined participation.*
Randomization	*If participants were not allocated into experimental groups, state so OR describe how participants were allocated to groups, and if allocation was not random, describe how covariates were controlled.*

Ecological, evolutionary & environmental sciences study design

All studies must disclose on these points even when the disclosure is negative.

Study description	*Briefly describe the study. For quantitative data include treatment factors and interactions, design structure (e.g. factorial, nested, hierarchical), nature and number of experimental units and replicates.*
Research sample	*Describe the research sample (e.g. a group of tagged Passer domesticus, all Stenocereus thurberi within Organ Pipe Cactus National Monument), and provide a rationale for the sample choice. When relevant, describe the organism taxa, source, sex, age range and*

any manipulations. State what population the sample is meant to represent when applicable. For studies involving existing datasets, describe the data and its source.

Sampling strategy	Note the sampling procedure. Describe the statistical methods that were used to predetermine sample size OR if no sample-size calculation was performed, describe how sample sizes were chosen and provide a rationale for why these sample sizes are sufficient.
Data collection	Describe the data collection procedure, including who recorded the data and how.
Timing and spatial scale	Indicate the start and stop dates of data collection, noting the frequency and periodicity of sampling and providing a rationale for these choices. If there is a gap between collection periods, state the dates for each sample cohort. Specify the spatial scale from which the data are taken
Data exclusions	If no data were excluded from the analyses, state so OR if data were excluded, describe the exclusions and the rationale behind them, indicating whether exclusion criteria were pre-established.
Reproducibility	Describe the measures taken to verify the reproducibility of experimental findings. For each experiment, note whether any attempts to repeat the experiment failed OR state that all attempts to repeat the experiment were successful.
Randomization	Describe how samples/organisms/participants were allocated into groups. If allocation was not random, describe how covariates were controlled. If this is not relevant to your study, explain why.
Blinding	Describe the extent of blinding used during data acquisition and analysis. If blinding was not possible, describe why OR explain why blinding was not relevant to your study.

Did the study involve field work? ☐ Yes ☐ No

Field work, collection and transport

Field conditions	Describe the study conditions for field work, providing relevant parameters (e.g. temperature, rainfall).
Location	State the location of the sampling or experiment, providing relevant parameters (e.g. latitude and longitude, elevation, water depth).
Access and import/export	Describe the efforts you have made to access habitats and to collect and import/export your samples in a responsible manner and in compliance with local, national and international laws, noting any permits that were obtained (give the name of the issuing authority, the date of issue, and any identifying information).
Disturbance	Describe any disturbance caused by the study and how it was minimized.

Reporting for specific materials, systems and methods

We require information from authors about some types of materials, experimental systems and methods used in many studies. Here, indicate whether each material, system or method listed is relevant to your study. If you are not sure if a list item applies to your research, read the appropriate section before selecting a response.

Materials & experimental systems

n/a	Involved in the study
☐	☒ Antibodies
☒	☐ Eukaryotic cell lines
☒	☐ Palaeontology
☐	☒ Animals and other organisms
☐	☒ Human research participants
☒	☐ Clinical data

Methods

n/a	Involved in the study
☒	☐ ChIP-seq
☒	☐ Flow cytometry
☐	☒ MRI-based neuroimaging

Antibodies

Antibodies used	Goat Polyclonal Anti-TPH2: Abcam, Cat# ab111828;dilution 1:500 Rabbit Polyclonal anti-5-HT1ARs: Abcam, Cat#ab85615; dilution 1:200 Mouse Polyclonal anti-5-HT1ARs: Millipore, Cat#MAB11041; dilution 1:400 Rabbit Polyclonal anti-VGLUT2; Millipore, Cat#MAB5504A4; dilution 1:500 Goat Polyclonal anti-SOM: Santa Cruz, Cat# sc-7819;dilution 1:500 Rabbit Polyclonal anti-c-Fos; Santa Cruz, Cat#sc-271243; dilution 1:500 Rabbit Polyclonal anti-5-HT2ARs; Abcam, Cat#ab66049; dilution 1:200
Validation	Anti-TPH2 (e.g. PMID: 28847002) anti-5-HT1ARs (Abcam, e.g. PMID: 30541912) anti-5-HT1ARs (Millipore, e.g. PMID: 29921169) anti-VGLUT2 (e.g. PMID: 22684983)

anti-SOM (e.g. PMID: 25869033)
anti-c-Fos (e.g. PMID: 29056294)
anti-5-HT2ARs (e.g. PMID: 30793039)

Eukaryotic cell lines

Policy information about cell lines

Cell line source(s)	*State the source of each cell line used.*
Authentication	*Describe the authentication procedures for each cell line used OR declare that none of the cell lines used were authenticated.*
Mycoplasma contamination	*Confirm that all cell lines tested negative for mycoplasma contamination OR describe the results of the testing for mycoplasma contamination OR declare that the cell lines were not tested for mycoplasma contamination.*
Commonly misidentified lines (See ICLAC register)	*Name any commonly misidentified cell lines used in the study and provide a rationale for their use.*

Palaeontology

Specimen provenance	*Provide provenance information for specimens and describe permits that were obtained for the work (including the name of the issuing authority, the date of issue, and any identifying information).*
Specimen deposition	*Indicate where the specimens have been deposited to permit free access by other researchers.*
Dating methods	*If new dates are provided, describe how they were obtained (e.g. collection, storage, sample pretreatment and measurement), where they were obtained (i.e. lab name), the calibration program and the protocol for quality assurance OR state that no new dates are provided.*

☐ Tick this box to confirm that the raw and calibrated dates are available in the paper or in Supplementary Information.

Animals and other organisms

Policy information about studies involving animals; ARRIVE guidelines recommended for reporting animal research

Laboratory animals	C57BL/6J mice (#213) purchased from Charles River used inthis study; GAD2-ires-Cre (#028867), CaMKII-ires-Cre (#005359), SOM-ires-Cre (#013044), CR-ires-Cre (#010774), PV-ires-Cre (#008069), Pet1-ires-Cre (#012712) male mice purchased from Jackson Laboratories were used in this study
Wild animals	The study did not involve wild animals.
Field-collected samples	This study did not involve samples collected from the field.
Ethics oversight	All animal protocols were approved by the Animal Care and Use Committee of the University of Science and Technology of China.

Note that full information on the approval of the study protocol must also be provided in the manuscript.

Human research participants

Policy information about studies involving human research participants

Population characteristics	Twenty-two chronic pain patients with depression, twenty-seven depressed patients without chronic pain, twenty-seven healthy control, and twenty-nine chronic pain without depression subjects were finally included in present study. There were no differences between groups in the terms of age (45.00±12.43 for chronic pain patients with depression; 38.19±10.46 for depressed patients without chronic pain; 40.41±7.30 for healthy controls; 32.76±13.02 for chronic pain without depression), or gender (6 male, 16 female for chronic pain patients with depression; 8 male and 19 female for depressed patients without chronic pain; 11 male and 16 female for depressed patients without chronic pain; 12 male and 17 female for chronic pain without depression).
Recruitment	We recruited patients from the First Affiliated Hospital of Anhui Medical University (Hefei, China) diagnosed with major depressive disorder according to the fourth edition of the Diagnostic and Statistical Manual of Mental Disorders (DSM-IV). Diagnosis was made by two psychiatrist (if one patient was diagnosed differenty, this patient would be exclued).The exclusion criteria for all participants included a current or past history of alcohol or drug dependency, pregnancy, neurological disorders, and any contraindications to fMRI scans.
Ethics oversight	This study was approved by the ethics committee of the First Affiliated Hospital of Anhui Medical University and was conducted in agreement with the principles set forth in the Declaration of Helsinki.

Note that full information on the approval of the study protocol must also be provided in the manuscript.

Clinical data

Policy information about clinical studies

All manuscripts should comply with the ICMJE guidelines for publication of clinical research and a completed CONSORT checklist must be included with all submissions.

Clinical trial registration	*Provide the trial registration number from ClinicalTrials.gov or an equivalent agency.*
Study protocol	*Note where the full trial protocol can be accessed OR if not available, explain why.*
Data collection	*Describe the settings and locales of data collection, noting the time periods of recruitment and data collection.*
Outcomes	*Describe how you pre-defined primary and secondary outcome measures and how you assessed these measures.*

ChIP-seq

Data deposition

☐ Confirm that both raw and final processed data have been deposited in a public database such as GEO.

☐ Confirm that you have deposited or provided access to graph files (e.g. BED files) for the called peaks.

Data access links *May remain private before publication.*	*For "Initial submission" or "Revised version" documents, provide reviewer access links. For your "Final submission" document, provide a link to the deposited data.*
Files in database submission	*Provide a list of all files available in the database submission.*
Genome browser session (e.g. UCSC)	*Provide a link to an anonymized genome browser session for "Initial submission" and "Revised version" documents only, to enable peer review. Write "no longer applicable" for "Final submission" documents.*

Methodology

Replicates	*Describe the experimental replicates, specifying number, type and replicate agreement.*
Sequencing depth	*Describe the sequencing depth for each experiment, providing the total number of reads, uniquely mapped reads, length of reads and whether they were paired- or single-end.*
Antibodies	*Describe the antibodies used for the ChIP-seq experiments; as applicable, provide supplier name, catalog number, clone name, and lot number.*
Peak calling parameters	*Specify the command line program and parameters used for read mapping and peak calling, including the ChIP, control and index files used.*
Data quality	*Describe the methods used to ensure data quality in full detail, including how many peaks are at FDR 5% and above 5-fold enrichment.*
Software	*Describe the software used to collect and analyze the ChIP-seq data. For custom code that has been deposited into a community repository, provide accession details.*

Flow Cytometry

Plots

Confirm that:

☐ The axis labels state the marker and fluorochrome used (e.g. CD4-FITC).

☐ The axis scales are clearly visible. Include numbers along axes only for bottom left plot of group (a 'group' is an analysis of identical markers).

☐ All plots are contour plots with outliers or pseudocolor plots.

☐ A numerical value for number of cells or percentage (with statistics) is provided.

Methodology

Sample preparation	*Describe the sample preparation, detailing the biological source of the cells and any tissue processing steps used.*
Instrument	*Identify the instrument used for data collection, specifying make and model number.*
Software	*Describe the software used to collect and analyze the flow cytometry data. For custom code that has been deposited into a community repository, provide accession details.*

Cell population abundance	*Describe the abundance of the relevant cell populations within post-sort fractions, providing details on the purity of the samples and how it was determined.*
Gating strategy	*Describe the gating strategy used for all relevant experiments, specifying the preliminary FSC/SSC gates of the starting cell population, indicating where boundaries between "positive" and "negative" staining cell populations are defined.*

☐ Tick this box to confirm that a figure exemplifying the gating strategy is provided in the Supplementary Information.

Magnetic resonance imaging

Experimental design

Design type	Resting state
Design specifications	Null
Behavioral performance measures	Null

Acquisition

Imaging type(s)	Functional imaging
Field strength	3T
Sequence & imaging parameters	Functional scans used a standard echo planar imaging sequence with the following parameters: repetition time/echo time ratio = 2000/22.5 ms, flip angle= 30 degrees, 33 slices, thickness/gap ratio = 4.0/0.6 mm, voxel size = 3.4 × 3.4 × 4.6 mm3, matrix size = 64 × 64, field of view = 220 × 220 mm2. T1-weighted anatomic images were acquired in sagittal orientation with three-dimensional inversion recovery prepared fast spoiled gradient recalled sequence (repetition time/echo time ratio = 8.676/3.184 ms, inversion time = 800 ms, flip angle= 8 degrees, field of view = 256 × 256 mm2, matrix size = 256 × 256, slice thickness= 1mm, voxel size = 1 × 1 × 1 mm3, sections = 188).
Area of acquisition	Whole brain scan

Diffusion MRI ☐ Used ☒ Not used

Preprocessing

Preprocessing software	The Data Processing Assistant for Resting-State fMRI toolkit (DPARSF) was used for image preprocessing. The first 10 volumes were discarded, the remaining volumes were processed using the following steps: slice timing correction, realignment, normalization using EPI templates resampled at a resolution of 3 × 3 × 3 mm, spatial smoothing (4 mm full width at half maximum), linear detrending, temporally bandpass-filtered (0.01 - 0.1 Hz). We defined the signal of white matter, the cerebrospinal fluid signal, the global signal and twenty-four Friston motion parameters as nuisance regressors to control for non-neuronal activation.
Normalization	The functional images were normalized to EPI templates resampled at a resolution of 3 × 3 × 3 mm.
Normalization template	EPI templates
Noise and artifact removal	White matter, the cerebrospinal fluid signal, the global signal and twenty-four Friston motion parameters as nuisance regressors
Volume censoring	Participants with excessive motion during scanning (> 3 mm in any direction, including angular motion) were excluded by manual operation.

Statistical modeling & inference

Model type and settings	mass univariate
Effect(s) tested	We just used ANOVA to test the effect of group

Specify type of analysis: ☐ Whole brain ☒ ROI-based ☐ Both

Statistic type for inference (See Eklund et al. 2016)	Cluster wise
Correction	Monte Carlo

Models & analysis

n/a	Involved in the study
☐	☒ Functional and/or effective connectivity
☒	☐ Graph analysis
☒	☐ Multivariate modeling or predictive analysis

Functional and/or effective connectivity: Pearson correlation

Graph analysis: *Report the dependent variable and connectivity measure, specifying weighted graph or binarized graph, subject- or group-level, and the global and/or node summaries used (e.g. clustering coefficient, efficiency, etc.).*

Multivariate modeling and predictive analysis: *Specify independent variables, features extraction and dimension reduction, model, training and evaluation metrics.*